POLITECNICO DI MILANO
DEPARTMENT OF MECHANICAL ENGINEERING
DOCTORAL PROGRAMME IN MECHANICAL ENGINEERING

LARGE EDDY SIMULATION OF WIND TURBINES:
INTERACTION WITH TURBULENT FLOW

Doctoral Dissertation of:
Paolo Schito

Supervisor:
Prof. Alberto Zasso
Prof. Fernando Porté-Agel

Tutor:
Prof. Gianpiero Mastinu

The Chair of the Doctoral Program:
Prof. Gianpiero Mastinu

Year 2011 – Cycle XXIV

I would like to express my gratitude to my supervisor Prof. Alberto Zasso for his support, his advice and curiosity during my research. I would like to thank also Dr. Daniele Rocchi for the suggestions and tips he gave me during these years.

I would like to thank Prof. Fernando Porté-Agel from École Polytechnique Fédérale de Lausanne for hosting me in the WIRE laboratory for five months and sharing with me his experience in the field of LES, atmospheric boundary layer and wind turbine modeling.

Nevertheless I would like to thank Prof. Carlo Bottasso from Dipartimento di Ingegneria Aerospaziale of Politecnico di Milano that gave me the full availability for sharing his wide experience in the modeling of wind turbines and provided the opportunity to do wind tunnel tests on the scaled wind turbine his research group, in particular Dr. Filippo Campagnolo, developed during these years.

I would like to mention the Department of Mechanical Engineering at the Politecnico di Milano that gave me the opportunity to fulfill my PhD, in particular the Dynamics and Vibrations section, the Wind Engineering group and the Wind Tunnel team. I would like to thank all people that gave me the opportunity to travel around the world to participate to many conferences, meetings and sharing experiences with other people.

My gratitude goes also to Dr. Raffaele Ponzini from CILEA that with his professional help and personal enthusiasm pulled me into the supercomputing universe.

A special mention goes to my "Tropical" colleagues Giacomo, Marco, Silvia, Vincenzo that shared with me almost the whole PhD adventure. A thought goes also to my colleagues Andrea, Egidio, Pietro, Antonio and to all MSc students with whom I worked together.

A want to remind my swiss italian friend Valerio for the great collaborations and support during office hours and free time.

A very special thank to my father, my mother and my brother and all my family for their support in all these years.

Last but not least I would like to mention Eva that bears, tolerates and sustains me since a long time with her love.

Abstract

WIND TURBINES are the most challenging subject in the renewable energy research area. The expansion of this technology within limited areas where the installation of wind turbines is profitable leads to the development of wind farms. In this configurations the close distance between the turbines produce an interaction between the wind turbine wakes that affects the wind energy harvesting and the loads on the wind turbine structure. The opportunity to model the interaction of the blades with turbulence structures and upwind rotor wakes helps understanding and take advantage of these effects on the turbine itself.

This work proposes an innovative actuator line method to model the interaction of the blade with the wind using Large-Eddy Simulation. The fundamental concept that lies in this approach is that a CFD framework provides the entire velocity field in the computational domain with a good accuracy: this information must be used to calculate the loads acting on the turbine blades and therefore to develop correctly the wake. Lifting line concept uses the angle of attack and relative velocity onto the blade to draw the lift and drag coefficients of the local airfoil from tabular curves that are known. The key issue is the correct evaluation of the angle of attack and velocity magnitude: common BEM approach uses induction factors on a reference wind to gather the angle, while the proposed approach estimates the angle and the air speed close to the blades using an "effective velocity" model.

The numerical results are compared with experimental wind tunnel tests in terms of thrust and torque performances of the wind turbine in different operating conditions and presenting the wake that is obtained.

Summary

THIS WORK aims to provide a numerical tool to predict the aerodynamic performances of a wind turbine in a turbulent wind or in the wake of an upstream turbine. This instrument is implemented using a Computational Fluid Dynamics (CFD) approach using Large Eddy Simulation (LES): this is the state of the art model for turbulent atmospheric boundary layer flows.

Chapter 1 introduces the background of this work, giving an introduction on the techniques used to study wind turbines and on the current numerical and experimental research activities

The wind turbine model using an actuator line approach is described in Chapter 2, calculating the wind turbine loads using the tabular aerodynamic characteristics of the blade sections and inserting the forces acting on the different sections of the wind turbine blades directly on the flow.

A new method is presented for the calculation of the aerodynamic forces using the actuator line approach: the proposed "effective velocity" model employs the velocity calculated close to the blade section to calculate the loads on the blade, while state-of-the-art methods use a reference velocity corrected with the BEM induction factors. The proposed model allows to reproduce the unsteady interaction of the blades with the incoming flow providing the correct interaction of the blade with the turbulence structures.

Chapter 3 presents an overview of literature methods for the generation of a turbulent flow, used for the BEM calculation in multibody studies of rotor loads or as input for transient CFD simulations. Large Eddy Simulation offers several possibilities for the reproduction of turbulent boundary layers; the geometrical reproduction of the experimental wind tunnel setup has been used, since previous work demonstrated that the unsteady loads on structures show a strong dependence on the flow turbulence characteristics, that can be correctly reproduced only by generating them in the correct way.

In Chapter 4 are presented the results of the numerical simulations for a uniform flow, compared with some preliminary wind tunnel test on a scaled wind turbine. The comparison is done in terms of thrust and torque at the rotor shaft and in terms of wind profiles in the wake of the wind turbine. The experimental wind tunnel tests and the numerical calculations show a good agreement, especially for high tip speed ratios with small blades angles of attack, when the blade section airfoils operate at a certain distance from stall condition.

LES simulations show their capability to reproduce the main features that characterize the flow around a wind turbine: it is possible to capture the typical vortical structures at the blade root (the hub vortex) and the vortices that leave the blade tips (the tip vortices), but also the wake of the hub and of the wind turbine tower. Turbulence intensity generated by the blades is well captured, while the hub effect on the wake is captured with less accuracy.

An example of a transitory wind turbine operation is provided, showing the transient performances due to a change in the blade pitch angle.

Chapter 5 presents the results for the interaction of the turbulent flow with the wind turbine. The wind tunnel incoming flow is reproduced with good agreement by LES calculations. Wind turbine thrust and torque performances are presented: again the agreement between experimental and numerical results is better for high tip speed ratios. The flow in the wake presents the characteristics that are expected in turbulent flow, with an evident effect of the mixing on the development of the wake downstream of the rotor.

This work has been supported by Regione Lombardia and CILEA Consortium through a LISA (Laboratory for Interdisciplinary Advanced Simulation) 2010-2011 grant.
(http://lisa.cilea.it)

Contents

List of Figures

CHAPTER 1

Introduction

THIS WORK wants to contribute to the modeling of the interaction of the rotor with the incoming flow. The possibility to perform wind tunnel tests on a wind turbine scaled model will not reproduce the full-scale machine operation, but gives the opportunity to test numerical methods with the control of the boundary conditions. The flow in the wind tunnel can be modeled in the numerical simulations and used to simulate the experimental test. The validation of the numerical approach will be done comparing the numerical results with experimental test; the verified code can be used to reproduce a full-scale operating condition by using an atmospheric boundary layer flow and the correct wind turbine geometric and aerodynamic features.

1.1 Historical remarks

Wind turbines are known since the 17^{th} century B.C. when Babylon was in his golden age: they are the oldest device to capture wind energy on land and Hammurabi used them for a big irrigation project. The first application of wind mills were in Sistan (Afghanistan) between the 7^{th} and the 9^{th} century A.D. where vertical axis wind turbines were built [17]. Windmills successively diffused in Asia, Middle East and Europe to grind corn and to pump water. In Europe the first horizontal axis wind turbines appeared in the 12^{th} century, as an alternative to watermills, located typically on the rivers that were property of nobility and clergy, giving an important resource to the new middle class. Wind mills, in addition, can work in any climate also when a very cold winter freezes the water.

The diffusion of electricity for industrial purposes in the second part of 18^{th} century gave the idea of using wind turbines to generate electrical power: the first wind turbine was built in Scotland in 1887 by Prof. James Blyth of Anderson's College and was

Table 1.1: *Annual installed new offshore wind turbine capacity (fully grid connected) [16]*

2008	2009	2010	2011
327MW	584MW	883MW	866MW

used to provide the electrical illumination to his cottage. One year later, in Cleveland (Ohio), Charles F. Brush realized a 17m rotor diameter wind turbine with 144 blades producing 12kW [29]. Small size wind turbines were widely produced for fuel saving and farm application until 1973, when the first oil crisis induced the world to look for alternative energy sources.

The research and development of new materials, technologies and engineering brought to the realization of the first multi-megawatt wind turbine in 1978: the 54 m rotor diameter "Tvindkraft" windmill was constructed and financed by a group of schools of Tvind (Denmark), to show an alternative to nuclear power, that was at the time an attractive power source. This wind mill has a quite modern design and is still working after nearly 34 years. The oil crisis lasted until 1987, when the largest wind turbines had a rotor diameter of 100m and a nominal power of 3.5MW.

In early 21st century global warming, fossil fuel reserves and energy security stimulated the interest in renewable energies. Since 2003 the wind energy industry is expanding at a rate of 30% per year: beside classical inland deployment, the offshore shallow water wind turbines are being more and more developed and energy investors are pushing for the installation of offshore wind farms [37]. Fukushima nuclear power plant disaster in 2011 gave new motivations to wind energy research and the actual efforts are directed toward floating offshore wind turbine technologies.

A press release by EWEA [16] states that despite the current economic crisis the "*EU offshore wind power market remained stable in* 2011"[1], since 235 new wind turbines, with a total power capacity of 866MW, were fully grid connected across nine wind farms (see Table 1.1). Actually offshore installed wind farms produce more that 3800MW with 1371 wind turbines in 53 wind farms; the currently under construction wind farms will bring online additional 2375MW. The target for EU installed offshore wind power capacity in 2020 is 40000MW, about the 4% of the EU's total electricity consumption.

1.2 Wind Turbines

The wind turbines of actual interest are the so-called "Horizontal-Axis Wind Turbines" (HAWT), which are the typical large scale Wind Energy framework. These machines are very complicated and advanced sets combining different fields: the most intuitive engineering branch which is involved is of course Aerodynamics, since the whole system is driven by the aerodynamic interaction between the wind and the blades. Also very important is the structural and the aero-elastic analysis of the entire machine, the mechanical and dynamical studies of all moving parts, the electrical energy conversion system and the economic survey of the investment.

Wind turbines are mainly studied with numerical methods, and it is not possible to attain a complete comparison with the data measured on full scale machines, since the

[1] EWEA – 19.01.2012 press release

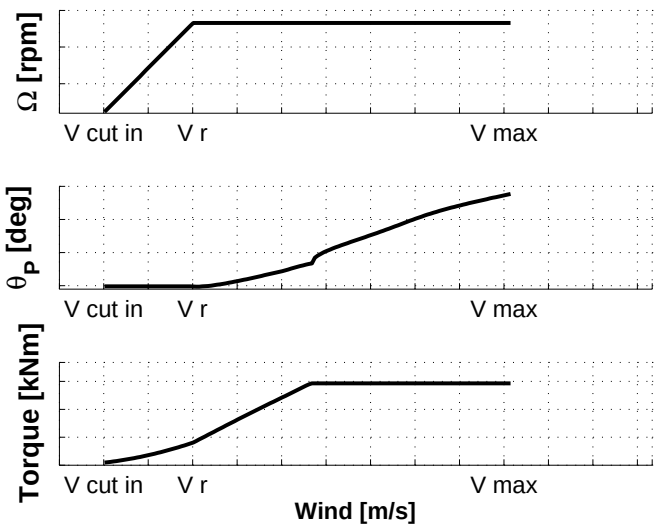

Figure 1.1: *Typical control law for a Horizontal Axis Wind Turbine. In the upper chart is presented the angular velocity as a function of incoming wind, on the center is reported the blade pitch angle as a function of the incoming wind and on the lower chart is presented the torque at the main shaft as a function of the incoming wind.*

aerodynamic boundary conditions are not fully known. It is possible to perform wind tunnel tests on wind turbine scaled models, but it is not possible to relate the model tests to a similar full scale wind turbine: Reynolds number ($Re = VL/\nu$), representing the ratio between inertial and viscous forces, has many orders of magnitude of difference if calculated for the model and the full scale rotor. Full scale Reynolds number is $Re > 10^6$, while wind tunnel tests may reach $Re \approx 3 \cdot 10^5$: the flow regime in these two cases is so different that the wind tunnel measurements cannot be referred to the full scale rotor. However there are many informations that can be obtained through wind tunnel tests in order to have a more detailed understanding of the physics of the wind turbine interaction with the wind.

Wind tunnel tests are mainly used for the verification of numerical methods using a model against model validation. A validated numerical code allows to calculate reliable results for the full scale simulations, given that the model assumptions are observed.

The essential features of wind turbines are treated in many text books ([17] [35] [37] [4]) and will be here briefly summarized, in order to provide a quick overview and get familiar with this subject.

1.2.1 Wind Turbine Operation

A wind turbine has a limited range of operation: the cut-in wind speed is about $3-5m/s$, the maximum operating speed is around $25m/s$. The control laws adjust the rotor speed and the blade pitch to the wind speed, in order to optimize the power output of the generator (see Figure 1.1). In this way the control system acts on the angle of attack in each section of the blade varying the corresponding load. This concept makes evident the importance of the aerodynamic study of the machine. The angle of attack and the air speed at each section of the blade of a wind turbine is the combination of

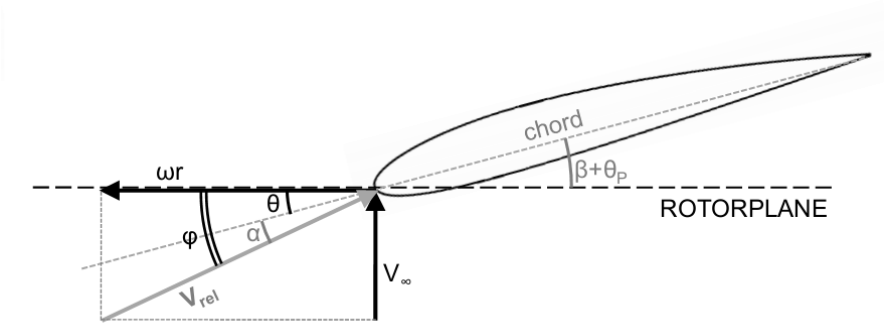

Figure 1.2: *Definition of aerodynamic angles on a blade's section airfoil. It is possible to identify the relative wind incidence angle with respect to the rotor-plane ϕ and the relative wind incidence angle to the airfoil α, the local twist β of the airfoil, the pitch of the blade θ_P that combined with β gives the local pitch θ of the airfoil.*

the incoming air speed (of course it is influenced by the presence of the turbine itself) and the rotational speed of the rotor (that depends on it's angular velocity and on the distance of the considered section from the rotor axis).

The relative wind incidence angle on each airfoil of the blade depends on the local wind angle and local rotational velocity and the design of the blade must take into account this native characteristic of the machine. Tip Speed Ratio (TSR) is defined as:

$$TSR = \Omega R / V_\infty \tag{1.1}$$

where Ω is the rotational speed of the rotor, R the radius of the wind turbine, V_∞ the undisturbed reference wind speed; it gives the information on the kinematics of the system. Different TSR give different kinematics of the system (that means different angles of attack) and therefore the blade design (airfoil, chord and twist distribution along the blade) must take into account all operating conditions: the design of a wind turbine is optimized for a certain site, monitoring the wind conditions in the installation place.

The control of a wind turbine, if the brake system is not used, acts substantially on the blade pitch angle that changes substantially the angles of attack between the blade local airfoil and the relative wind speed. In this way the wind incidence angle changes of a constant value on the entire blade generating a higher or lower driving force to speed up or slow down the rotor speed. In figure 1.2 it is possible to see how the different angles are combined. In general the local angle of attack of an airfoil is defined as:

$$\alpha = \phi - \theta = \phi - (\beta + \theta_P) \tag{1.2}$$

where ϕ is the relative wind incidence angle with respect to the rotor-plane, θ is the local blade pitch angle with respect to the rotor-plane, given by the sum of the local blade twist β and the blade pitch θ_P. In equation 1.2 it is evident that the blade pitch θ_P directly influences the angle of attack and hence the aerodynamic forces on the blade.

Given these basic informations on the mechanism of generating the forces on a wind turbine, it is possible to give a simple hint on the different control laws:

- stall regulated wind turbines are designed to reach stall and therefore loose lift force at a certain angle of attack (and therefore at a definite TSR) that coincides with the generator limit. This is the classical control law approach for wind turbines.
- pitch regulated wind turbines is a more recent technique, since it needs more technology to adjust the pitch angle of the blades during the turbine operation. The active pitch control allows to obtain almost any aerodynamic loading of the blades. In the last years an even more sophisticated approach controls the pitch of every single blade during the rotation, in order to optimize the power output when running in shear flow adjusting the pitch for the "instantaneous" TSR.
- active stall controlled wind turbines is a combination of the previous two concepts, since pitch regulation is used to stall the entire or part of the blade, obtaining a quick response of the turbine with small pitch regulations.

Turbine control is of growing importance with the increase of the rotor's size: their operation in the atmospheric boundary layer flow widely changes the local angles of attack of the blades during a single rotation, leading to power losses but also to loads that may cause fatigue damages to the entire machine [55].

1.3 Wind Turbine Wakes

A first distinction that is possible to perform on the wind turbine wakes, it is the definition of a "near wake" and a "far wake": the first extends lets say for three rotor diameters, the second extends to the wake's end. In the near wake it is possible to distinguish the peculiar characteristics of a wind turbine wake, while in the far wake only a generalized momentum deficit is noticeable. Of course this definition is quite general, since inflow conditions and tip speed ratio may affect these regions.

The near wake of a wind turbine is characterized by an helical structure that is expanding behind the rotor. The simple Betz assumptions describe correctly the wake expansion, while BEM theory, introducing the tangential induction factor a', gives information on the wake rotation. The rotation of the wake is in the opposite direction of the wind turbine rotation; this because of the transfer of angular momentum between flow and the rotor that produces the wake rotation and the aerodynamic torque generating the power output. Looking at the wake structures in more detail, it is possible to capture the tip vortex structure, which highlights the helical characteristic of the wake and the wake expansion. Vortical structures are not present only at the blade tip, but also at the blade root, with a different sense of rotation. This strong characterization of the wake becomes weaker moving downstream because of the fluid viscosity and gets mixed, until it is completely dissipated.

The far wake starts after the near wake and extents up to 10-15 rotor diameters. In this case is not possible anymore to recognize the wake structures, but the wake rotation and the momentum deficit are still present. It is possible to study the wake meandering phenomenon due to the interaction with the turbulent flow [21].

Near wake studies are important when analyzing the single wind turbine aerodynamics in normal operation, in yawed conditions or in extreme loading, since the correct modeling of the flow structure interaction can be evaluated in both structural loading

and in the reproduction of the correct wake. A correct replication of the wake is important for the study of the interaction between several wind turbines, since the wake of the upwind rotor is the input the downstream wind turbines.

1.4 Wind Turbine Modelling

Several models have been developed in the last century, starting with Lanchester (1915) and Betz (1920) to predict the maximum power output of an ideal wind turbine, until Glauert (1935) formulated the Blade Element Momentum (BEM) method that is still used at present days. Certainly this model has been upgraded to allow most complex and refined calculations, but it is the core of today's design codes.

Computational Fluid Dynamics (CFD) analysis of wind turbines is a very challenging purpose: the flow around a wind turbine is complex, presents many levels of detail, from the smallest boundary layer on the single blade to the atmospheric turbulent boundary layer wind interaction with the terrain orography. It is necessary to focus the target of the work to use properly the available resources: if the aim is the reproduction of the flow-blade interaction, it is better to focus on the modeling of the blade; if the interest is on the interaction between different turbines, the wake must be correctly reproduced dropping the small detail of the blade boundary layer.

A typical approach when modeling a wind turbine in CFD is the Actuator Disk (AD) method or the Actuator Line (AL) method: the wind turbine is geometrically reproduced in the computational domain but its actions on the flow are introduced as external forcing in the Navier-Stokes equations. The calculated forces rely on the incoming flow and act on the fluid itself. The forces are calculated using the local aerodynamic lift and drag coefficients of the blade profiles, since the geometry of the wind turbine is not reproduced.

Using AD methods the forces can be constant all over the disk area [25] or be transient, depending on the local inflow [56]. In both examples the simulation reproduces a momentum deficit in the wake of the wind turbine that is proportional with the thrust force of the wind turbine. It is of course possible to include the rotational effect on the flow, using a rotating actuator disk [56]. A more refined method, but also more computationally demanding, is the AL model presented by Sørensen and Shen [53], that calculates the loads on the blades of the wind turbine. With this approach, it is possible to evaluate accurately the loads along the blade and therefore the resulting flow-field is more detailed and reproduces the peculiar features of a wind turbine wake.

There is a key issue in all the calculations performed using the AD and AL technique: the airfoil data, used to calculate the aerodynamic loads, must be correct and the reference velocity used for the evaluation of the local velocity and angle of attack must be meaningful for the phenomenon under study. At a first glance this can result trivial, but in reality it is the most critical and decisive issue. Some studies on this topics have been conducted by Shen et al. [49] and Cadei [5]

In the last years interest in wind tunnel modeling of wind turbines has grown [48]: some big European (MEXICO[2] [47] and MEXNEX(T)[3]) and American (UAE[4]) projects have been financed to perform wind tunnel tests on wind turbines.

[2]MEXICO – Model Rotor Experiments In Controlled Conditions – ECN 2001-2006
[3]ECN 2008-2014 – www.mexnext.org
[4]NREL Unsteady Aerodynamics Experiment

In this topic is focused also the research of Politecnico di Milano, where some works have been carried out on the interaction of wind turbines wakes by Zasso et al. [58] [60], some research on offshore wind turbines by Bayati [1], the testing of control laws and aeroelastic response by Bottasso et al. [3]. A more detailed work focused on the wind farms wake interaction has been done by Porté-Agel et al. [9] [8] [10] [20].

Full scale wake measurements for the validation of wind tunnel tests and CFD calculations are performed by LiDAR measurement by Iungo et al. [22]

1.5 Incoming Flow Modelling

Incoming flow modeling plays an important role on both the wind tunnel tests and the numerical calculationsn, since it is responsible of the machine loading. IEC 61400 rules [18] prescribe the standard prescriptions that the numerical atmospheric wind profiles must take into account for the calculations on full-scale wind turbines. These rules define both the mean (steady) and fluctuating (unsteady) part of the wind components. As a matter of fact it is of primary importance to correctly define the inflow: when referring to full-scale machines the incoming flow characteristics are influenced by terrain surface roughness (uniform distribution of obstacles/trees/bushes, etc...), by big structures and obstacles (hills, buildings, etc...) that may affect the machine loads and power production. Numerical simulations of wind turbines are usually conducted on a fully developed boundary layer: appropriate boundary conditions may be calculated in analytical form for steady calculations (see Richards and Hoxley [44] and Blocken et al. [2]) or can be calculated with dedicated simulations. When simulating a turbulent boundary layer flow the most suitable approach is LES, where the Navier-Stokes equations are filtered. In this framework the large eddies that are present in the flow are explicitly calculated, while the smaller ones (typically smaller than the size of the grid) are modeled with a Sub-Grid Scale (SGS) model. LES calculations use the assumption of the Energy Cascade theory, that states that the turbulent kinetic energy contained in the large eddies is transferred to the smaller eddies up to the smallest scale, where it is dissipated. The SGS model reproduces the smallest scales and the dissipation that has a quite universal formulation.

When the phenomenon under study is strongly connected with the turbulence present in the flow, it is important that the turbulent structures are correctly reproduced: for this reason many approaches have been developed in order to take into account the correct fluctuations, mixing and advections induced by turbulent flows. The simplest models are spectral synthesizer, developed by Kraichnan [28] and refined by Smirnov et al. [51], that are used as a perturbation method on a mean inflow, specifying the desired turbulence intensity I and characteristic length scale L. Another approach, especially designed for a wind energy purpose, proposed by Mann [33] [34] and widely diffused at DTU use a body force as a function of the desired turbulence intensity and length scale to create the turbulent structures. Besides these simple and computationally cheap methods, the wind engineering community that exploit a LES approach to turbulence problems uses periodic domains in order to develop the correct flow characteristics, using geometrical obstacles ([38] [39]) or rough wall functions ([43] [56] [31]). With these methods it is necessary to run a preliminary simulation in order to obtain a transient time-history of turbulent flow to be used as boundary condition for the calculation

of interest. Other approaches use re-scaling of the solution in a plane at some distance from the inlet using it, opportunely rescaled, as inlet boundary condition for the numerical simulation itself. Best results in reproducing the atmospheric turbulent boundary layer flows are obtained by Porté-Agel et al. [42] and Porté-Agel [41] that with his pseudo-spectral code is able to reproduce all the main features of the stable/unstable atmospheric boundary layer.

CHAPTER 2

Actuator line solver

THE ACTUATOR LINE model literature review and the specific model used in this work are presented. The assumptions of the model are analyzed, in order to develop a model suitable for the interaction of the rotor with the turbulence structures of a boundary layer flow. A new "effective velocity" model, for the interaction of the blades with the local wind speed is proposed in order to provide a reliable interaction of the rotor with the flow turbulence structures. This AL model reproduces not only the blade forces on the flow, but models also the hub and the pylon interaction with the incoming wind, giving a detailed description of the interaction of the entire machine with the wind. The solver is implemented in the open source OpenFOAM environment solving Large Eddy Simulation (LES) equations with the introduction of the actuator line loads.

2.1 Actuator line model

Actuator line models are a more refined version of the actuator disk concept. The basis of those models is the Blade Element Momentum theory (BEM). A good review of the actuator disk methods can be found in Wu and Porté-Agel [56] that is based on the model presented by Sørensen and Shen [53]: actuator disk distribute all over the rotor area the axial and eventually the tangential force acting on the wind turbine and, for this reason, AD is suitable for steady calculations. AL is more complex, the rotation of the blades must be reproduces and therefore it has an unsteady formulation. This approach is widely used also for structural analysis of wind turbines, since it does not need a complete reproduction of the flow field, but only the unsteady time histories upstream of the turbine.

There are several assumptions on the BEM theory summarized by Snel [52]:

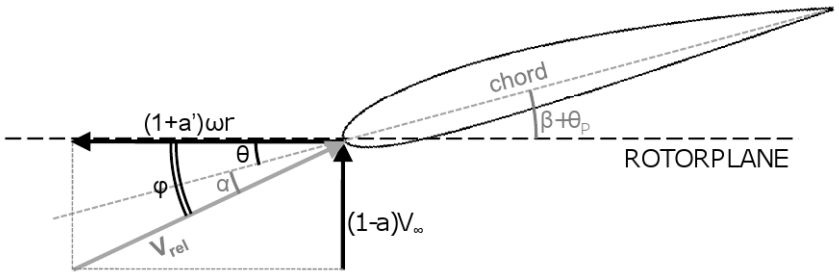

Figure 2.1: *Definition of the velocities calculated with BEM approach. The difference with respect to Figure 1.2 is in the values of the axial and tangential velocities.*

- **the flow is steady state and non-turbulent**: it is obvious that this statement is not correct for real wind turbines;
- **the flow is axial symmetric**: this is probably very close to reality in case of uniform flow field, but generally is not true;
- **2D sectional flow on the blades**: this is an assumption that is not true, since turbulent flows and stalled flows are always three-dimensional;
- **no dynamic effects**: this is neglected since it is very difficult to quantify and model the dynamic stall of the different sections.

Of course the common AL approach is widely used for many purposes in wind turbine calculation, since it is a reliable approach, and some simple modifications can be done to get suitable results for CFD turbulent boundary layer simulations. The simplest methods use a reference velocity to calculate the aerodynamic forces, that is the mean wind speed at hub height (Jimenez et al. [25]). This is a good model for steady inflow with uniform velocity and it is in good agreement with the AL assumptions. Other methods use the vertical mean velocity profile to calculate the rotor forces: this method reproduces the unsteady loading of the turbine due to the shear in the boundary layer, but it does not fulfill the hypothesis of axial-symmetric flow. Other models use the unsteady wind velocity upwind of the rotor to calculate the blade forces. BEM theory is not valid for these kind of flows since the main assumption is that the flow in a given annulus of the rotor does not affect the flow at the adjacent annuli. Let's take a look at the BEM theory and successively to the new effective velocity model.

2.1.1 Blade Element Momentum theory

Many papers and books propose the Blade Element Momentum (BEM) theory, which here will be only quickly presented in order to make some comments on the theory. The main concept of this theory is that the presence of the rotor induces some variations in the incoming undisturbed flow field and, in particular, an *axial induction* or axial deceleration of the air and a *tangential induction* or rotation of the flow that are identified with an axial induction factor a and a tangential induction factor a'. The induction

factors depend on axial C_N and tangential C_T force coefficients as can be seen in:

$$a = \frac{1}{\frac{4\sin^2\phi}{\sigma(r)C_N} + 1} \tag{2.1}$$

$$a' = \frac{1}{\frac{4\sin\phi\cos\phi}{\sigma(r)C_T} - 1} \tag{2.2}$$

where ϕ is the wind incidence angle of attack with respect to the rotor plane as reported in figure 2.1 calculated as:

$$\phi(r) = \frac{(1-a)V_\infty}{(1+a')\omega r} \tag{2.3}$$

and $\sigma(r)$ is the local solidity of the rotor, calculated as:

$$\sigma(r) = \frac{c(r)B}{2\pi r} \tag{2.4}$$

where r is the distance of the considered point from the hub, V_∞ is the undisturbed wind velocity, $c(r)$ is the local chord and B the number of blades that form the turbine. The induction factors vary with the position along the blade. Of course a and a' influence C_N and C_T so the determination of the induction factors is an iterative process. The axial and tangential force coefficient are defined as:

$$C_N = \frac{F_N}{\frac{1}{2}\rho V_{rel}^2 c} \tag{2.5}$$

$$C_T = \frac{F_T}{\frac{1}{2}\rho V_{rel}^2 c} \tag{2.6}$$

$$\tag{2.7}$$

but can also be defined as:

$$C_N = C_L\cos\phi + C_D\sin\phi \tag{2.8}$$

$$C_T = C_L\sin\phi - C_D\cos\phi \tag{2.9}$$

The classic calculation of aerodynamic forces on an airfoil is typically given as:

$$L = \frac{1}{2}\rho V_{rel}^2 c C_L \tag{2.10}$$

$$D = \frac{1}{2}\rho V_{rel}^2 c C_D \tag{2.11}$$

while the relation between the forces in the airfoil reference and the rotor plane reference is:

$$F_N = L\cos\phi + D\sin\phi \tag{2.12}$$

$$F_T = L\sin\phi - D\cos\phi \tag{2.13}$$

Of course this model gives good results for steady flow, but for unsteady flows or shear flows the methodology is disputable.

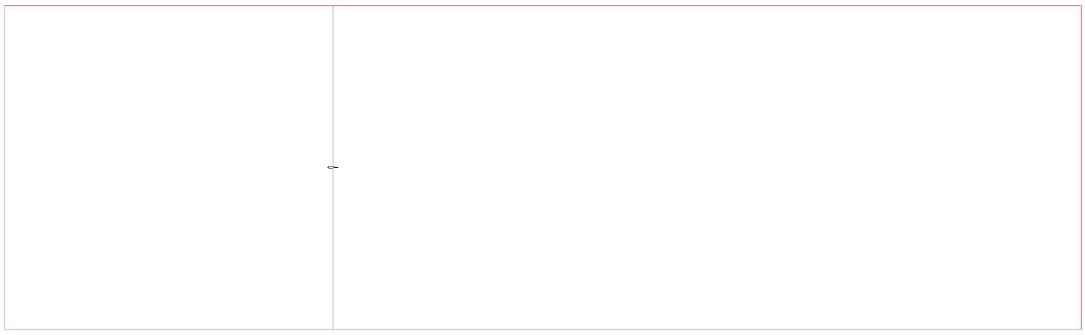

Figure 2.2: *Domain of the 2D CFD simulation for the calculation of the airfoil perfomance. The line on which the flow velocity and angle data are gathered is indicated.*

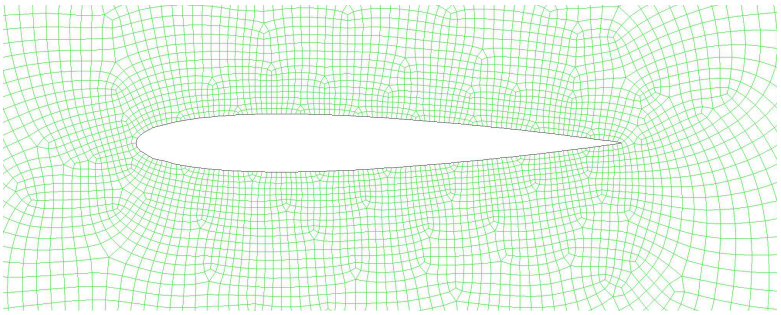

Figure 2.3: *Mesh around the NACA0012 airfoil used for the CFD simulations.*

2.1.2 Effective velocity model

CFD approach to wind turbines gives almost all data that are needed for the calculation of the forces on the rotor; for this reason it is worth to use all the information that the numerical simulation is able to give.

The discussion is on the way the reference velocity and angle of attack are obtained in order to calculate the aerodynamic forces: LES simulations offer a detailed description of the flow field. Current actuator line models calculate the blade forces in turbulent flows using as reference the undisturbed velocity the wind speed at rotor height [43] or at some distance upstream of the rotor plane [56] to get the reference velocity. It is not possible to say if the velocity in the chosen position is not affected by the presence of the turbine or if the aerodynamic forces are calculated with that wind speed represents the correct load on the turbine: there is at least a time shift in the applied loads and several rotor turns, depending on the TSR at which the turbine is operating. In any case the mean aerodynamic forces acting on the flow field are rather correct, but the result is similar to what can be calculated using the reference vertical mean wind profile. The turbine loads calculated in this way are similar to the approach used by standard structural calculations, since the reference velocity is taken more or less as a separate input and the rotor is not interacting properly with the flow.

A very simple model has been developed to correlate the local wind incidence angle with the undisturbed reference angle of attack: the attempt is to reproduce a more suitable interaction of the wind turbine blades with the turbulent structures in the flow. The model has been calibrated realizing bi-dimensional simulations of a NACA0012

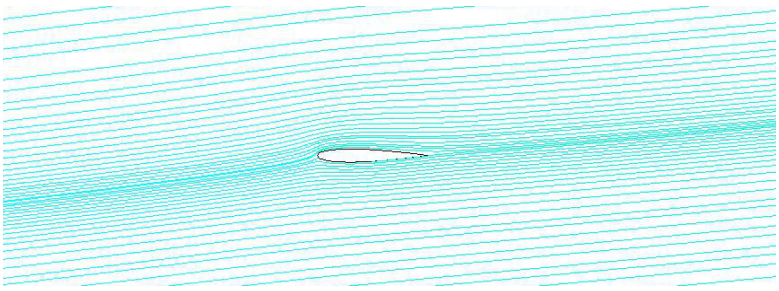

Figure 2.4: *Pathlines around the NACA0012 airfoil for an angle of attack of* $\alpha_\infty = 6°$.

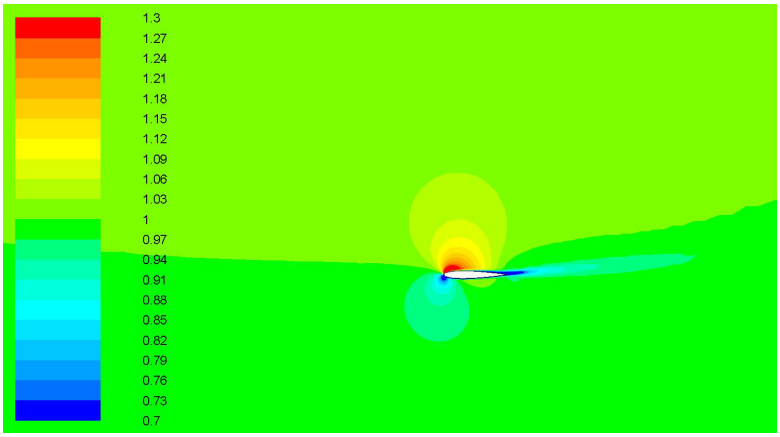

Figure 2.5: *Non-dimensional velocity magnitude field v around the NACA0012 airfoil for an angle of attack of* $\alpha_\infty = 6°$.

airfoil at different angles of attack. The typical angles of attack for a section of a blade is $0 < \alpha < 10$. For this reason the numerical simulations have considered three conditions: $\alpha_\infty = 3°,6°,9°$. All numerical simulations use the same mesh, reported in Figure 2.3, and the angle of attack is changed with different boundary conditions. The pathlines for the simulation of the NACA0012 profile at 6° angle of attack are reported in Figure 2.4. In order to have non-dimensional quantities the local velocity has been divided with the reference velocity magnitude V_{ref}, obtaining the non-dimensional velocity magniture v_i in each cell as:

$$v_i = \frac{V_i}{V_{ref}} \tag{2.14}$$

where V_i is the velocity in each cell. A plot of v_i can be seen in Figure 2.5: the air is faster near the suction surface (the upper side of the profile) while a lower wind speed is present at the pressure surface. As can be seen the perturbation of the unperturbed wind speed extends at some distance from the airfoil, especially on the upper side of the wing profile. In a similar manner, a non-dimensional wind incidence angle α_i^* has been defined as:

$$\alpha_i^* = \frac{\alpha_i - \alpha_\infty}{\alpha_\infty} \tag{2.15}$$

in this case it is possible to see that the influence of the airfoil on the α^* is higher than what has been seen for the non-dimensional velocity magnitude v. The same considerations can be done for the wind incidence angles $\alpha_\infty = 3°$(Figure 2.7) and

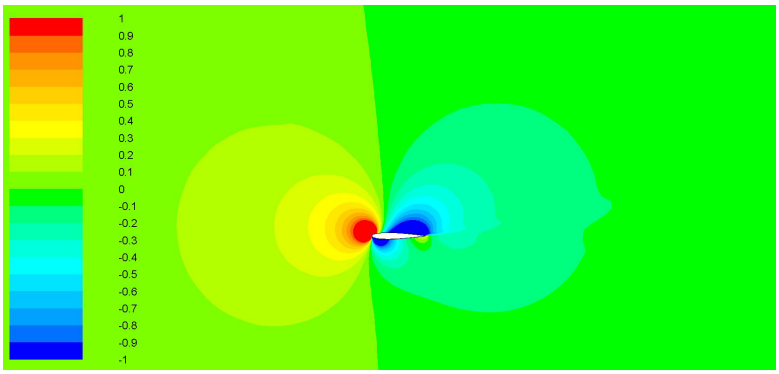

Figure 2.6: *Non-dimensional angle of attack α^* field around the NACA0012 airfoil for an angle of attack of $\alpha_\infty = 6°$.*

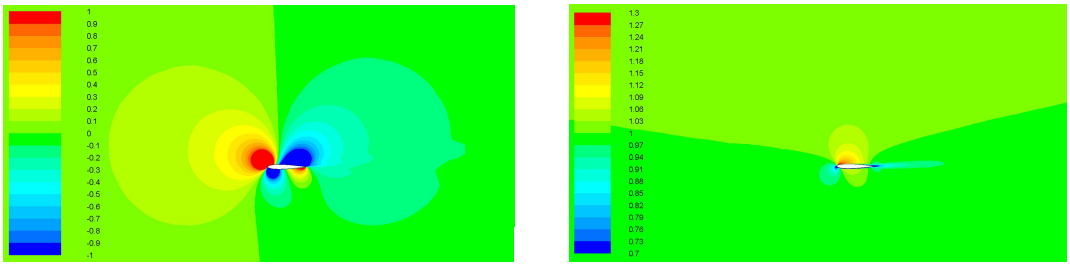

Figure 2.7: *Non-dimensional angle of attack α^* (left) and non-dimensional velocity magnitude v (right) around the NACA0012 airfoil for an angle of attack of $\alpha_\infty = 3°$.*

$\alpha_\infty = 9°$(Figure 2.8).

The calculation of the mean value of the angle of attack α' and non-dimensional velocity magnitude V' has been done considering a line perpendicular to the airfoil through the mid point of the chord, reported in Figure 2.2. The distance from the airfoil is reported in non-dimensional distance d/c, where d is the distance of the point from the airfoil and c is the chord of the wing profile. The plots show that there is only a minor dependence of α^* with the undisturbed angle of attack α_∞, since the differences are visible at very close distance from the airfoil. The non-dimensional velocity magnitude v^* shows a clear dependence from α_∞, because increasing the wind incidence angle increases also v^* close to the airfoil.

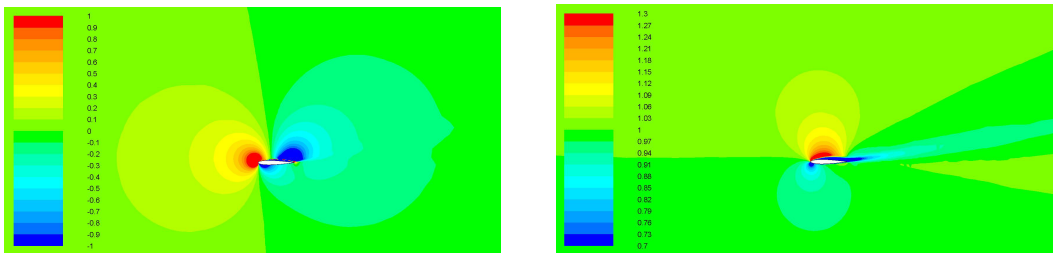

Figure 2.8: *Non-dimensional angle of attack α^* (left) and non-dimensional velocity magnitude v (right) around the NACA0012 airfoil for an angle of attack of $\alpha_\infty = 9°$.*

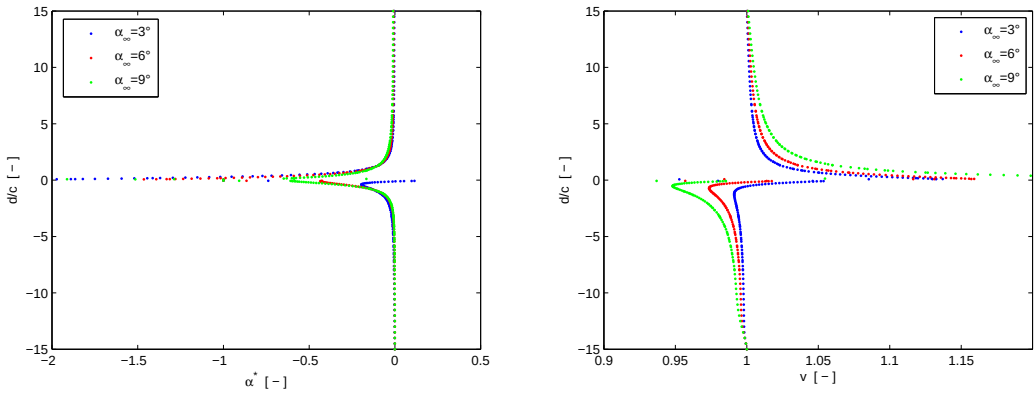

Figure 2.9: *Non-dimensional angle of attack α^* (left) and non-dimensional velocity magnitude v (right) along the airfoil chord perpendicular line. The plots are reported for incidence angles $\alpha_\infty = 3°,6°,9°$.*

The mean value of velocity magnitude V'_L and mean angle of attack α'_L are calculated on the line perpendicular to the profile chord (see Figure 2.2) for different intervals L expressed in non-dimensional distance d/c (see Figure 2.10). The non-dimensional angle of attack α^* the non-dimensional mean angle of attack α'_L is defined as:

$$\alpha'_L = \frac{\alpha_L}{\alpha_\infty} \tag{2.16}$$

where α_L is the mean angle of attack in the considered interval. When calculating the mean values the interval used is expressed in non-dimensional distance d/c from the airfoil chord: the interval considers all the points p in the region $-d/c \leqslant p \leqslant d/c$. The mean velocity and the mean angle of attack have been related to the undisturbed reference wind speed and direction finding a relation for different angles of attack. The idea is to use a reference line as short as possible across the rotor plane, in order to have the mean value closer to the local effective velocity. As can be seen in Figure 2.10 the results in terms of non-dimensional mean velocity V' is not very sensitive to the interval length used to calculate the mean value and, as can also be seen in Figure 2.9 the main differences are due to the differences between the suction and pressure side of the airfoil. In the three proposed wind incidence angles the non-dimensional mean velocity $V' \approx 1$. Looking at the mean non-dimensional angle of attack α' the result is different: the angle shows an evident influence of the interval length used to calculate the mean value.

The choice of a reference number for α' needs to take into account the requests of the model: give a relationship between the reference angle of attack α_∞ and the local mean value α' and have the smallest interval in order to capture the local flow fluctuations. A reasonable value for the mean non-dimensional angle of attack can be $\alpha' = 0.75$, that has a good correspondence for a range of non-dimensional distances $5 \leqslant -d/c \leqslant 10$.

When comparing this range of non-dimensional distances with a distance with respect to the rotor plane, this can be expressed as a distance of a quarter of a rotor radius R: tipically the ratio of a blade length R with the maximum chord c_{max} is $R/c_{max} \approx 15$, while a good estimate of the ratio of the blade length with the blade mean chord c_{mean} is $R/c_{mean} \approx 25$.

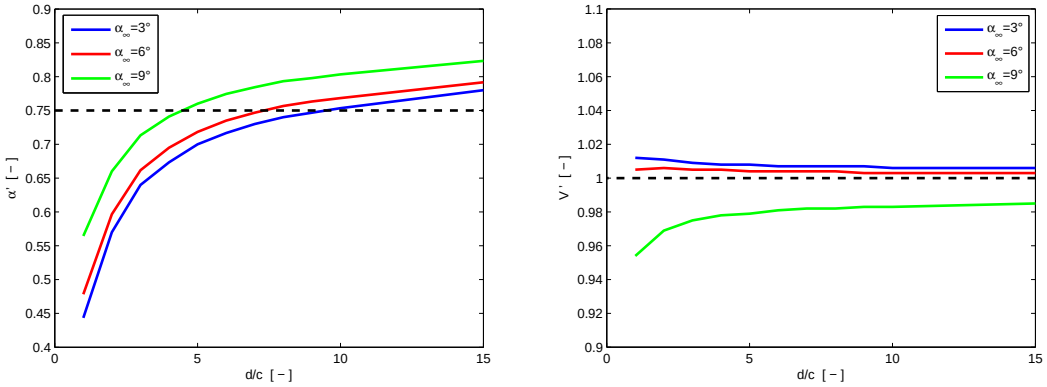

Figure 2.10: *Non-dimensional mean angle of attack α' (left) and non-dimensional mean velocity magnitude V' (right) along the airfoil chord perpendicular line calculated for different line lengths. The plots are reported for incidence angles $\alpha_\infty = 3°,6°,9°$. The black dashed line is the value used as reference.*

This considerations helps to assess that a reasonable distance d for the calculation of the mean values is $d = 0.25R$, leading to a mean value of non-dimensional distance

$$\frac{d}{c_{mean}} = 0.25\frac{R}{c_{mean}} = 6.25 \tag{2.17}$$

that satisfies the considerations previously done.

Finally it is possible to define the effective velocity model constants that are used to convert the local incidence angle α' to the reference incidence angle α_∞ and the local velocity V' to the reference velocity V_∞:

$$\alpha' = 0.75\alpha_\infty \tag{2.18}$$

$$V' = 1.0V_\infty \tag{2.19}$$

The method doesn't need to perform any correction for axial or tangential induction correction factors, since this operation is performed by the solver that calculates the flow in the whole domain.

2.2 Solver structure

The solver is built in the free open source OpenFOAM® [40] framework. The version used for this work is OpenFOAM v1.7.1. OpenFOAM is a partial differential equation tool that uses a finite volume approach to solve Navier-Stokes equations.

2.2.1 LES solver

The code is written in *C++*, an object oriented programming (OOP) language. The writing of the equations in the code is quite simple, because the top-level code is very intuitive. The implementation of Navier-Stokes equations:

$$\frac{\partial \rho \mathbf{U}}{\partial t} + \nabla \cdot \rho \mathbf{U}\mathbf{U} - \nabla \cdot \mu \nabla \mathbf{U} = -\nabla p \tag{2.20}$$

can be written as:

```
solve
(
    fvm::ddt(rho, U)
  + fvm::div(phi, U)
  - fvm::laplacian(mu, U)
    ==
  - fvc::grad(p)
);
```

In this piece of code it is very easy to recognize the single terms reported in equation 2.20, since using an OOP language it is possible to simplify the readability of the code, defining methods to access the variables and hiding unwanted very complex pieces of code. Due to the flexibility of the code, some additional classes have been defined in order to include the actuator line model in the solver.

The standard solver for incompressible transient flow named *pisofoam* is modified for the introduction of the actuator line forces. This solver is suitable also RANS equations, but in this case it is used for LES. The filtered equation that is used is:

$$\frac{\partial \overline{\mathbf{U}}}{\partial t} + \nabla \cdot \overline{\mathbf{U}}\overline{\mathbf{U}} - \nu \nabla^2 \overline{\mathbf{U}} + \mathbf{f} = -\nabla \overline{p} \tag{2.21}$$

where $\mathbf{f}$ is the volume force introduced by the actuator line, and named `VolumeForce` in the code. The filtered advection term $\nabla \cdot \overline{\mathbf{U}}\overline{\mathbf{U}}$ requires the knowledge of the exact solution since it is nonlinear, but, since it is not possible to know the exact solution, it needs the modeling of the nonlinear part of this term, using a Smagorinsky model, obtaining the following equation:

$$\frac{\partial \overline{\mathbf{U}}}{\partial t} + \nabla \cdot \overline{\mathbf{U}}\,\overline{\mathbf{U}} + 2\nu_{eff} \nabla (\nabla \overline{\mathbf{U}} + (\nabla \overline{\mathbf{U}})^T) + \mathbf{f} = -\nabla \overline{p} \tag{2.22}$$

What is written in the solver code is the following:

```
solve
{
    fvm::ddt(U)
  + fvm::div(phi, U)
  + turbulence->divDevReff(U)
  + VolumeForce
    ==
  - fvc::grad(p)
};
```

the term that contains the Sub-Grid Scale (SGS) model is written in the `turbulence->divDevReff(U)` function and contains:

$$2\nu_{eff} \nabla (\nabla \overline{\mathbf{U}} + (\nabla \overline{\mathbf{U}})^T) \tag{2.23}$$

where the effective viscosity ν_{eff} is given by the sum of the eddy viscosity ν_{sgs} and the kinematic viscosity of the fluid ν:

$$\nu_{eff} = \nu + \nu_{sgs} \tag{2.24}$$

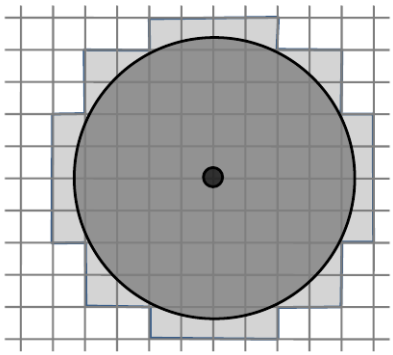

Figure 2.11: *Schematics of the actuator disk region. The light gray cells are investigated for line forces, the gray circle describes the rotor area, the dark gray circle evidences the hub area.*

and the eddy viscosity ν_{sgs} is given by:

$$\nu_{sgs} = (C_S \triangle)^2 (\nabla \overline{\mathbf{U}} + (\nabla \overline{\mathbf{U}})^T) \tag{2.25}$$

where $\triangle$ is the grid size and $C_S = 0.1678$ the Smagorinsky constant for isotropic turbulence.

An important osservation that can be done on the code is that, unlike other works ([56], [53], [24], [36]), the forcing term is introduced directly on the grid because a finite volumes approach is used, and the code suffers no instabilities: the force can be applied on a single location, while the other approaches use a regularization kernel to smear the actuator line forces on the neighbor nodes.

2.2.2 Actuator line solver

The calculation of the actuator line forces is done separately between the time-steps. The code runs in parallel using MPI.

A new *C++* class named `actuatorLineExplicit` is defined with associated variables and methods. As can be inferred from the class name, the forced introduced are calculated explicitly, meaning that the forces introduced in the calculation at the time-step $[t+1]$ use teh flow variables at the current timestep $[t]$. The forces on the blades are calculated with the approach presented in section 2.1.2 using equations 2.18 and 2.19. In addition forces are calculated on the hub and on the tower using the same approach, using a drag coefficient $C_D = 1$. At a first trial, all cells having a part that intersects the disk region, as can be seen in figure 2.11 are marked: the light-gray region cells may have a force induced by the turbine, the gray region is the analytical and physical zone where the rotor is, while the dark-gray region is the zone relative to the hub forces. The forces are introduced in the cells that are intersected by the actual position θ_{blade} of the blades, calculated as:

$$\theta_{blade} = \omega t + (n-1)\frac{2\pi}{3} \tag{2.26}$$

where ω is the rotation speed of the turbine, t is the elapsed time and $n = 1,2,3$ is the blade number. In figure 2.12 the cells that are intersected by the actuator line and that will have a forcing term are highlighted. The forcing due to the portion of line that

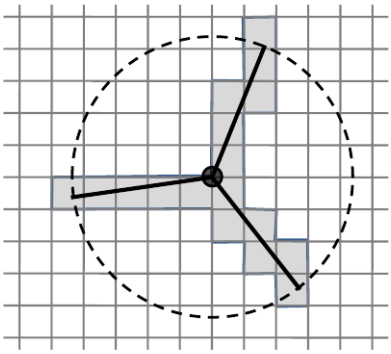

Figure 2.12: *Schematics of the actuator line region. The forces are introduced in the highlighted cells.*

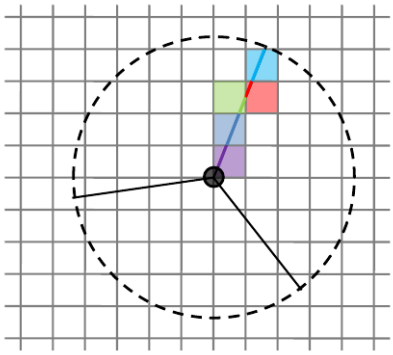

Figure 2.13: *Schematics of the actuator line: a single line is splitted in one segment per cell; each segment is responsible for the forcing in the corresponding cell.*

intersects the cell is applied only on the cell itself as can be seen in figure 2.13: the forcing calculated on the blue line is put on the blue cell, the forcing due to the red line is applied on the red cell and the force calculated on the green line is applied on the green cell. This is a first order approximation, since the force is applied directly on the cell without evaluating the distance of the line from the neighbor cells. A possible improvement may be the splitting of the actuator line force between the adjacent cells. In figure 2.14 there are indicated the most important geometric details that are used to compute the forces of the actuator line. The segment $\overline{ab}$ with length l_{ab} generates a force that is applied in the point E: the forces are calculated for the point 1, that is the middle point of the segment, where all blade parameters necessary for the calculation (the radial distance r to determine the rotational speed, the blade section twist $\theta(r)$, the chord $c(r)$, the airfoil characteristics $C_D(r,\alpha)$, $C_L(r,\alpha)$) are evaluated. The reference velocity is calculated on the cell center E. The same can be stated for the segment $\overline{bc}$ with length l_{bc}, where the forces calculated for point 2 are placed in A, for segment $\overline{cd}$ with length l_{cd}, where the forces calculated for point 3 are placed in B and so on. The calculation of the effective velocity is implemented along a line parallel to the rotor axis that intersects the cell centers as can be seen in figure 2.15: the method is described in section 2.1.2 and the mean velocity $\overline{\mathbf{V}}_C$ is calculated as:

$$\overline{\mathbf{V}}_C = \frac{\mathbf{V_B} + \mathbf{V_C} + \mathbf{V_D}}{3} \tag{2.27}$$

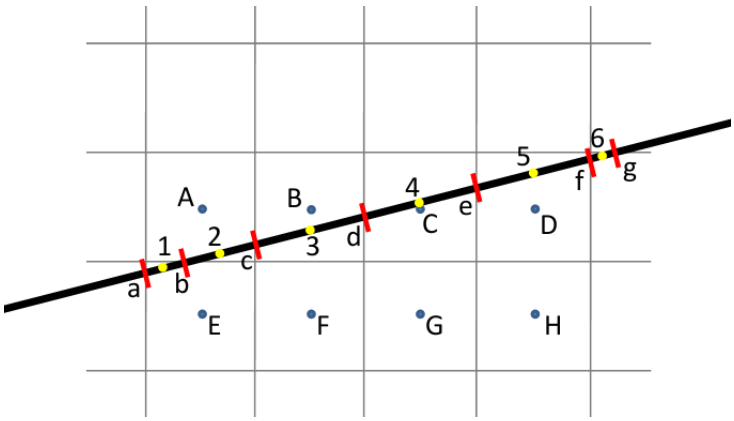

Figure 2.14: *Detail of the actuator line: the uppercase letters point out the cell centers, the lowercase letters show the intersection of the line with the cell borders and the numbers the center of the segments of the line.*

It is possible to fix an interval to be used for the calculation of the mean velocity: in the model the interval is $L = 0.5R$ symmetrically distributed upwind and downwind the wind turbine, so the velocity is taken up to $0.25R$ upwind and $0.25R$ downwind. The assumptions made in the effective velocity model are respected, since the typical blade chord-radius ξ are:

$$\xi = \frac{R}{c} \approx A \qquad with \;\; 20 < A < 40 \tag{2.28}$$

this means that taking the distance $L = 0.25R$ the reference distance-chord ratio ζ is consistent with what defined in section 2.1.2 having $5 < \zeta < 10$. Of course the mean wind speed $\overline{\mathbf{V}}$ is a vector, and in this case it is possible to make a vector sum to calculate the relative velocity $\mathbf{V_{rel}}$ to the blade section:

$$\mathbf{V_{rel}} = \overline{\mathbf{V}} + \omega \mathbf{r} \tag{2.29}$$

The decomposition of $\mathbf{V_{rel}}$ in axial, tangential and radial direction:

$$\mathbf{V_{rel}} = V_A \mathbf{a} + V_T \mathbf{t} + V_R \mathbf{r} \tag{2.30}$$

where $\mathbf{a}$ is the axial direction, constant for all points, $\mathbf{t}$ and $\mathbf{r}$ are the tangential and radial direction that change with the angular position of the blade. The angle ϕ with respect to the rotor-plane can be calculated as:

$$\phi = \arctan(\frac{V_A}{V_T}) \tag{2.31}$$

From the geometric characteristics of the rotor is possible to choose the correct value of local chord c and twist β. Using the relation 1.2 and looking to figure 1.2, it is possible to define the relative wind incidence angle α' as:

$$\alpha' = \phi - \beta - \theta_B \tag{2.32}$$

remembering that θ_B is the pitch of the blade. Not all necessary terms are known yet, since the aerodynamic force coefficients to be used must be referred to the *effective velocity*: the angle of attack that is used to find the aerodynamic lift and drag coefficients

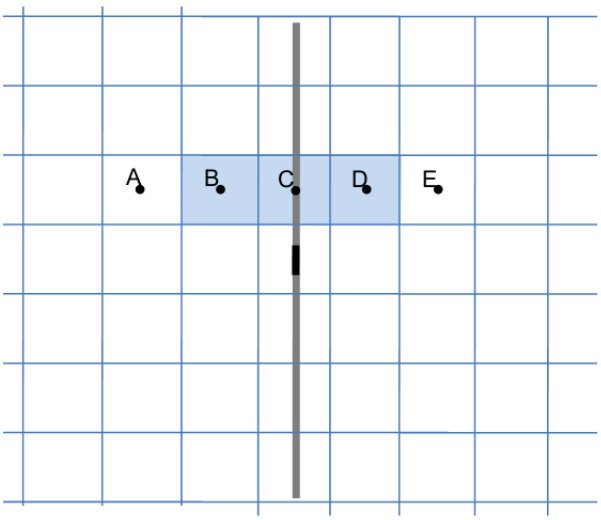

Figure 2.15: *Numerical implementation of the calculation for reference velocity. The considered plane is perpendicular to the rotor-plane.*

is not α' but α and, remembering equation 2.18 it is possible to write:

$$\alpha = \frac{\alpha'}{0.75} \tag{2.33}$$

$C_L(\alpha)$ and $C_D(\alpha)$ curves of the airfoil in the considered section are defined in tabular aerodynamic data, it is necessary to define a tip loss correction to take into account of the loss of circulation near the blade tip. The method used is the Glauert approximation to Prandtl tip loss function TLC [50] given by:

$$TLC = \frac{2}{\pi}\arccos(e^{-\frac{N(R-r)}{2r\sin\phi}}) \tag{2.34}$$

where $N = 3$ is the number of blades, R the wind turbine radius, r the local distance from the hub and ϕ the angle between the local relative velocity and the rotor plane. At this point the calculation of the lift $\mathbf{L}$ and drag $\mathbf{D}$ for the given cell is calculated as:

$$\mathbf{L} = TLC\frac{1}{2}\rho V_{rel}^2 clC_L\mathbf{l} \tag{2.35}$$

$$\mathbf{D} = \frac{1}{2}\rho V_{rel}^2 clC_D\mathbf{d} \tag{2.36}$$

where c is the local chord, l the length of the segment of the actuator line that passes through the cell (as reported in 2.14), $\mathbf{l}$ and $\mathbf{d}$ are the unit vectors of lift and drag force: $\mathbf{d}$ has the same direction of the relative velocity component but is perpendicular to the actuator line direction $\mathbf{r}$, while $\mathbf{l}$ is perpendicular to both $\mathbf{d}$ and $\mathbf{r}$. The force that is passed to the Navier-Stokes equation reported in 2.22 is a force per unit volume and is given by:

$$\mathbf{f} = \frac{\mathbf{L}+\mathbf{D}}{V} \tag{2.37}$$

where V is the volume of the cell.

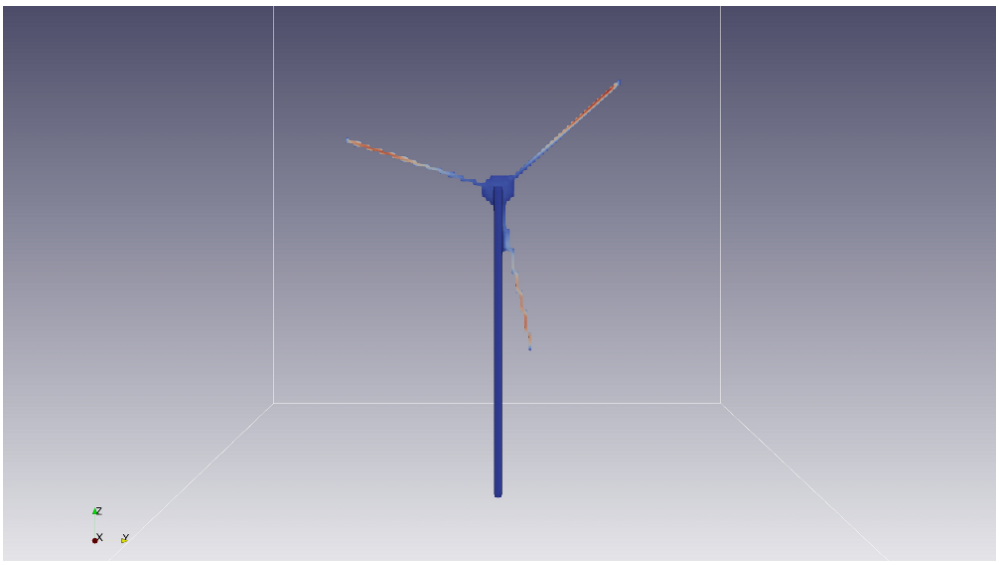

Figure 2.16: *Turbine description by the inserted volume forces in the domain. Red color means higher forces, blue lower forces*

In Figure 2.16 it is possible to see the result of this model: the surface that contains the forces introduced on the flow represent the wind turbine geometry. It is possible to identify the geometry of the tower, the nacelle and the three blades. The color of the surface is representative of the loads: the pylon and the nacelle are blue, since they generate low forces, while the blades generate stronger forces and the color changes to red in the region where the highest loads are reached.

CHAPTER 3

Turbulence Generation

TURBULENCE
"*the most important unsolved problem of classical physics*"[1]

WIND TURBINES operate in open fields, on top of a mountain or in the middle of the sea, and there is no concern on the operating condition: the main target in wind energy is to extract as much power as possible. Of course the design of wind turbines is optimized to the wind conditions of the installation site, that include average wind speed and direction at hub height, mean wind and turbulence intensity vertical profiles. The reproduction of the wind is very difficult since it's characteristics are affected by the features of the pursued path. To overcome this problem IEC 61400 [18] defined the method to calculated the reference wind that must be used to reproduce the unsteady incoming wind characteristics of a specific site. This approach is widely used for the BEM calculations used for the aero-servo-elastic simulations of wind turbines, that are the state-of-the-art for the structural and performance calculations of wind turbines. The calculation of turbine performances with real wind depends on the correct reproduction of the atmospheric boundary layer (ABL) and the same can be asserted for wind tunnel tests on scaled models of wind turbines: the performances of the numerical model rely on the correct reproduction of the features of the wind tunnel flow.

3.1 Turbulent boundary layer generation methods

The generation of a turbulent boundary layer wind is a very difficult task in the wind engineering field: the generated flow must reproduce the atmospheric wind. This prob-

[1] Richard Phillips Feynman [1918–1988] – Nobel Prize in Physics in 1965

lem relates to many different aspects in wind energy: the wind turbine structure must stand with the most extreme conditions and the design of the blades must grant satisfying performances in all conditions. Other scientific communities face similar problems: hydrologists, meteorologists, bridge engineers, building engineers, pollution and particle dispersion communities need to model the interaction with the atmospheric boundary layer. The usual approach is the modeling of a fully developed boundary layer [54], where it can be neutral (either considering or not the temperature gradients), but also stable and unstable ABL are studied. Wind tunnel studies are performed on scaled models in order to investigate the interaction of the model with the wind. Wind tunnel turbulence generation theory has been formulated by Irwin [19]. The development of numerical codes that need to be validated against experimental tests need to model the unsteady flow. In the following sections will be presented the experimental and numerical methods for the generation of turbulent flows.

3.1.1 Wind Tunnel Turbulence Generation

The typical characteristic of a Boundary Layer Wind Tunnel is the length of the testing chamber [7]. The most important facilities have a length to height ratio of at least $10:1$, in order to have enough space to develop the BL. The characteristics in terms of mean velocity, turbulence intensity and integral length scale vertical profiles [12] are usually obtained placing passive turbulence generators at the beginning of the test section and distributed floor roughness [19]. The big turbulent structures produced by the spires take the flow to the desired conditions, enhancing the turbulence production in order to arrive quicker to the target flow.

The gradient in mean wind speed vertical profile depends on the fluid viscosity and on the friction velocity: for this reason it is important to put the correct floor roughness on the ground. The shape of the floor roughness can be very different between the different wind tunnels: in Tokyo Polytechnic University[2] the floor roughness is made of small cubes or parallelepipedes, in Von Karman Institute[3] the floor roughness consists of cylindrical obstacles, while in Politecnico di Milano[4] the floor roughness is represented by pyramids.

3.1.2 CFD Turbulence Generation

The definition of the correct boundary conditions, when running calculations of turbulent boundary layer flows, is never an easy task: typically transient boundary conditions must be imposed. A primitive approach suggests that should be modeled anything that enhances or dissipates the turbulence: this method implies the choice of the features to be modeled and the usage of a very large number of points to reproduce details that could be neglected if a different system can be used. The methods commonly used to generate unsteady fluctuations in the flow can be identified in four categories:

- *random noise*: on the mean velocity profile a random noise is added with an amplitude proportional to the turbulence intensity. However the characteristics of a turbulent flow are not those of a random noise;

[2] Wind Engineering Research Center directed by prof. Yukio Tamura and prof. Ahsan Kareem
[3] Environmental and Applied Fluid Dynamic Department supervised by prof. Jeroen van Beeck
[4] Dipartimento di Meccanica, supervised by prof. Alberto Zasso

- *synthetic methods*: the velocity fluctuations on the mean velocity profile are generated from an inverse Fourier transform of a given spectrum obtaining the correct power spectral density and spatial correlation. A method was proposed by Kondo [27], another one has been proposed by Druault et al. [14] using Proper Orthogonal Decomposition (POD) and Linear Stochastic Estimation (LSE). Another method has been proposed by Xie and Castro [57], while a method typically used for wind energy applications has been proposed by Mann [34];
- *preliminary simulation*: this technique allows to split the problem in two different steps: the first simulation reproduces only the generation of a turbulent flow and is therefore a calculation that is focused on this point, while the second simulation, that is conducted subsequently, is focused only on the fluid-structure interaction. The transient velocity time-history on a section of the domain is used as input for the second simulation ([30] [31]);
- *recirculation and rescaling*: these methods are the most diffused and have been introduced by Lund et al. [32], then Kataoka [26] revised it and Nozawa and Tamura [38] [39] simplified it. The calculation domain is divided in two regions: one is used like a periodic simulation, with rescaling of the result, where the output of the first region is re-introduced as input boundary condition for the same region; the second part of the domain is dedicated to the fluid-structure interaction.

In this work it has been used the precursor simulation method, because previous works pointed out that the wind induced loads are highly related to the turbulence characteristics of the flow: the comparison with experimental wind tunnel data must be done reproducing correctly the turbulent wind tunnel flow. An example of this can be found in Zasso et al. [59] and Rocchi et al. [45] [46], and will be described in the next section. The full paper can be found in Appendix 5.4.

3.2 Turbulent Boundary Layer Generation

The method that has been chosen is the preliminary simulation that accurately describes the turbulent structures of the flow and, in a second time, analyzes the interaction with the wind turbine. This approach has been found to be the most reproductive for the validation of CFD results against wind tunnel experimental tests: it is very difficult to get a fully developed boundary layers in wind tunnels and it must be stated that the flow that is obtained in wind tunnels depends on the setup used to generate the turbulence.

3.2.1 Turbulence generation: an example

An example of this can be found in Zasso et al. [59] and Rocchi et al. [45] [46], the full paper can be found at the end of the manuscript, where this aspect has been investigated in depth, with a specific application of wind engineering: wind loads on buildings and specifically the time history of static pressure on the building surface. The first considerations can be done on the experimental setup: in the Politecnico di Milano Wind Tunnel (Diana et al. [13]), the wind profile is obtained using large spires at the beginning of the boundary layer test section that generate a preliminary vertical wind profile and big turbulent structures [19]. The floor upwind the model is covered with roughness elements to provide the correct shear to the lower part of the boundary layer and

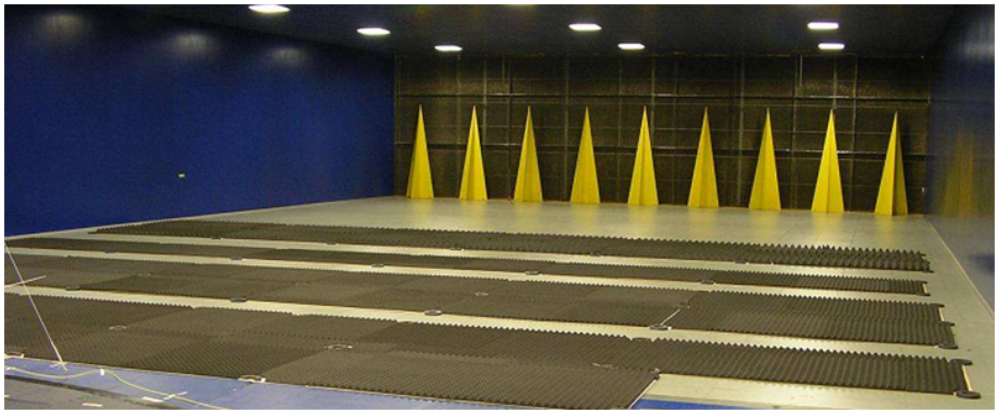

Figure 3.1: *Wind Tunnel setup with spires and floor roughness.*

enhances the production of turbulence close to the floor. This approach is used since Kolmogorov gave the definition of the energy cascade for turbulent flows, that supports this method for the turbulence generation in the wind tunnel: big spires produce large structures that will transfer their energy to smaller eddies until reaching the smaller isotropic and homogeneous scales (called Kolmogorov scales) where the energy is dissipated. This definition helps to understand that the turbulent flow is getting smoother moving downstream from the spires. The floor roughness transfers energy to the lower part of the boundary layer, in order to maintain the turbulence intensity and the vertical mean wind profile. In the wind tunnel, the boundary layer develops downwind of the spires and dissipates energy. This is different from what happens in full-scale, since the big structures in the atmospheric boundary layer are produced by the orography, by the obstacles and by convection. For this reason an accurate description of the wind tunnel flow can be done only doing a 1 to 1 CFD reproduction of the wind tunnel configuration. The experimental setup can be found in Rocchi et al. [46] and is shown in Figure 3.1. As already mentioned in section 3.1.1, it is possible to identify the elements that allow to generate the turbulent boundary layer. The big yellow spires generate a preliminary vertical profile and the big structures in the flow. Of course, the shadow effect of the spires is visible at close distance from them, but the turbulence diffusion allows to reduce and cancel this unwanted feature. Floor roughness enhances the shear stress on the ground and also the maintenance of the small scale turbulence near the floor. In this case the floor roughness is realized with pyramids of different sizes in order to achieve the desired mean wind profile, with the correct turbulence intensity and length scale. The same geometry is reproduced by the CFD computational domain, in order to get a numerical flow field consistent with the experimental one. The comparison of numerical and wind tunnel data can be seen in Figure 3.3. Numerical and experimental data show a good agreement in terms of mean wind profile, also in the lower part of the wind profile, that was very important for the specific application and is also a very difficult task for this kind of problems. The turbulence intensity I_x defined as reported in Dyrbye and Hansen [15]:

$$I_x(z) = 100 \cdot \frac{\sigma(x(z))}{\overline{U(z)}} \tag{3.1}$$

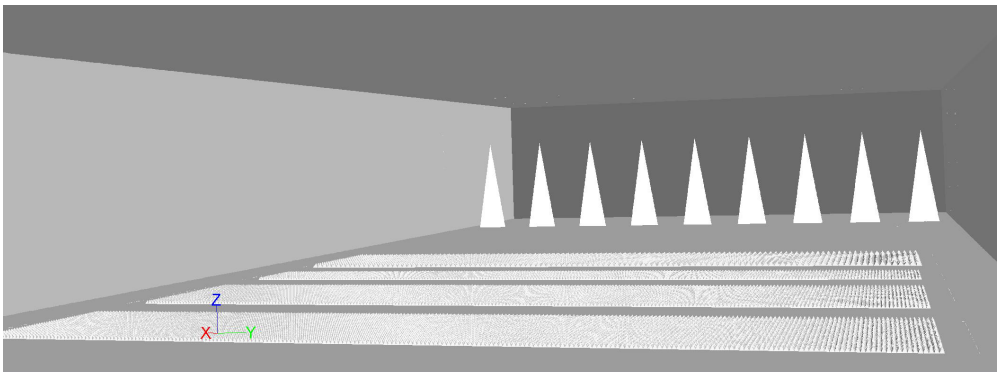

Figure 3.2: *CFD setup with spires and floor roughness.*

where $x = U(z), V(z), W(z)$ is the streamwise, lateral or vertical component of the time history in the considered point at height z, σ represents the standard deviation and $\overline{U(z)}$ is the mean streamwise velocity magnitude. The indication given by the turbulence intensity is on the magnitude of the fluctuations in the velocity. The prescription [15] for the relation between the different turbulence intensities is:

$$I_V(z) \approx 0.75 I_U(z) \qquad I_W(z) \approx 0.5 I_U(z) \tag{3.2}$$

As can be seen in Figure 3.3, the longitudinal turbulence intensity is higher than the other two though it is not exactly in the prescribed relationship; the vertical component is higher than the vertical one. The turbulence length scale is calculated as a function of the time scale $T_U(z)$ using the autocorrelation $\rho_U^T x(z,\tau)$ of the velocity time history $U(t,z)$ calculated as:

$$\rho_U^{Tx}(z,\tau) = \frac{1}{T}\int_0^T U(t+\tau,z)U(t,z)dt \tag{3.3}$$

where τ is the time delay. The definition of time scale $T(z)$ is:

$$T_U^x(z) = \int_0^\infty \rho_U^T(z,\tau)d\tau \tag{3.4}$$

and, finally, is possible to calculate the length scale L_U^x as:

$$L_U^x(z) = T_U^x(z)U(z) \tag{3.5}$$

It is evident that with this method it is possible, opportunely substituting the velocity direction in equation 3.3, to get only the L_U^x, L_U^y and L_U^z since it is not possible to get experimental data to verify the length scales using non longitudinal velocity components. Dyrbye and Hansen [15] define the typical relationships between the longitudinal, lateral and transversal length scales as:

$$L_V^x(z) \approx 0.3 L_U^x(z) \qquad L_W^x(z) \approx 0.2 L_U^x(z) \tag{3.6}$$

Figure 3.3 shows a satisfying agreement between the experimental and LES on the along-wind length scale, while numerical simulations overestimate the lateral and vertical length scales. In the work of Rocchi et al. [46] it seems that the along-wind length

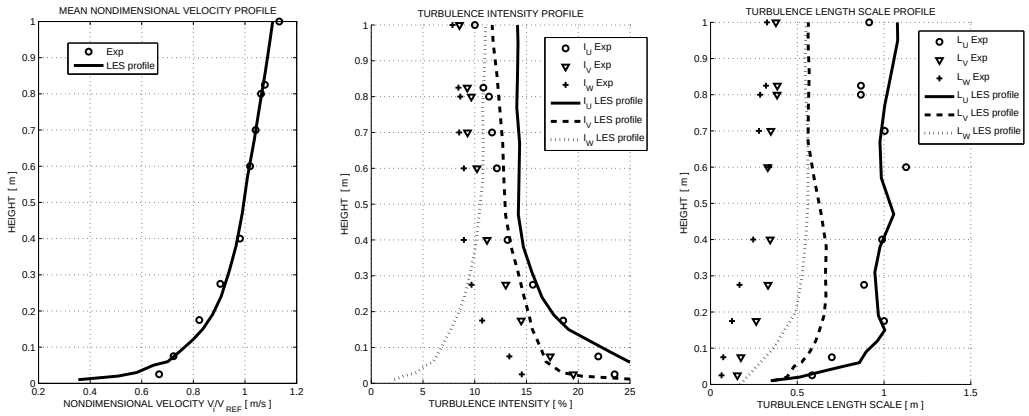

Figure 3.3: *Vertical Wind tunnel experimental and LES profiles in the considered configuration: mean wind speed (left), turbulence intensity (center), turbulence length scale (right).*

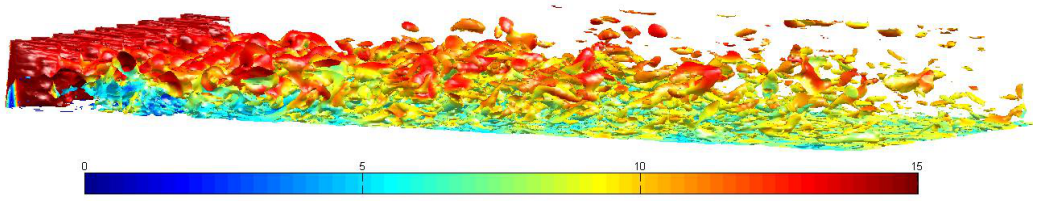

Figure 3.4: *Visualization of an instantaneous vorticity iso-surface of the wind tunnel flow field.*

scale is dominant for the generation of the pressure loads. In Figure 3.4 it is proposed a visualization of the turbulent structures that are present in the flow. It is possible to infer the position of the spires and the large turbulence structures in the flow close to the spires. The large eddies, generated by the spires, loose their energy and produce smaller eddies. As can be seen in the Figure, the structure of the turbulent structures becomes smaller and they are stretched in the longitudinal direction. This result is in agreement with the information given by the vertical profile of turbulence length scale reported in Figure 3.3.

The simulation, which has been realized with this empty wind tunnel channel, has been used to calculate the transient velocity-pressure distribution on a transversal plane, to be used as transient boundary condition for the successive LES analysis. The detailed results of this work can be found in Rocchi et al. [46].

3.3 Atmospheric Boundary Layer

Until now the discussion has been conducted on the generation of a boundary layer that must be of course reproductive of the full scale phenomenon. In this case Stull [54] gives the correct definition of boundary layer:

"We can define the boundary layer as that part of the troposphere that is directly

influenced by the presence of the earth's surface, and responds to surface forcings with a timescale of about an hour or less."

The effort done in this work is to develop and validate a scaled numerical model with scaled wind tunnel model tests. Of course, the wind generation methods cited in section 3.1 are not very accurate for the reproduction of wind tunnel flow, but aim to represent the full scale boundary layer flow. These methods are reproductive of the neutral boundary layer, but most critical flow conditions can be obtained by peculiar flows that are generated by stability or instability of the boundary layer, rather than surface roughness: this can be the case of the nocturnal jet that occurs at few tent's of meters aloft, generating highly skewed loads on the turbine. Usually wind turbines are loaded with a flow that increases the wind speed with height, while this particular case shows a high-speed jet at hub height or lower. Wind tunnel studies are conducted analyzing the influence of the stability of the boundary layer and can be found in Chamorro and Porté-Agel [9].

CHAPTER 4

Wind Turbine in uniform flow

LARGE EDDY Simulations on uniform flow using the actuator line model are compared to experimental data measured on the wind turbine wind tunnel models realized by prof. Bottasso [3]. The computational domain is reproductive of the low turbulence test section of the Politecnico di Milano Wind Tunnel. This gives the opportunity to have a direct comparison of the numerical results with the experimental data.

4.1 Wind Tunnel setup

In the experimental test the wind turbine has been placed at the beginning of the high-speed low-turbulence test section of the Politecnico di Milano Wind Tunnel. The wind turbine is installed on a 6 components balance at the beginning of the removable test chamber that is 4 meters wide, 3.8 meters high and 5 meters long. The wind turbine has a rotor-diameter of 2 meters and the tower is 1.9 meters high. The wake measurements have been done using hot-wire anemometers. Due to the short length of the low turbulence test section, it is possible to measure wind profiles only close to the rotor-plane and, in particular, at the non-dimensional distances $x/D = 0.5, 1.05, 1.6, 2.15$.

4.2 Numerical setup

CFD simulations have been conducted on a domain that is reproductive of the low turbulence test section of the Politecnico di Milano Wind Tunnel. The domain section where the turbine is placed is $3.8x4$m, as for the experimental test. The wind turbine is placed both horizontally and vertically in the center of the testing section. For this configuration the blockage is quite high, being the solid blockage $A/S = 0.01$, where

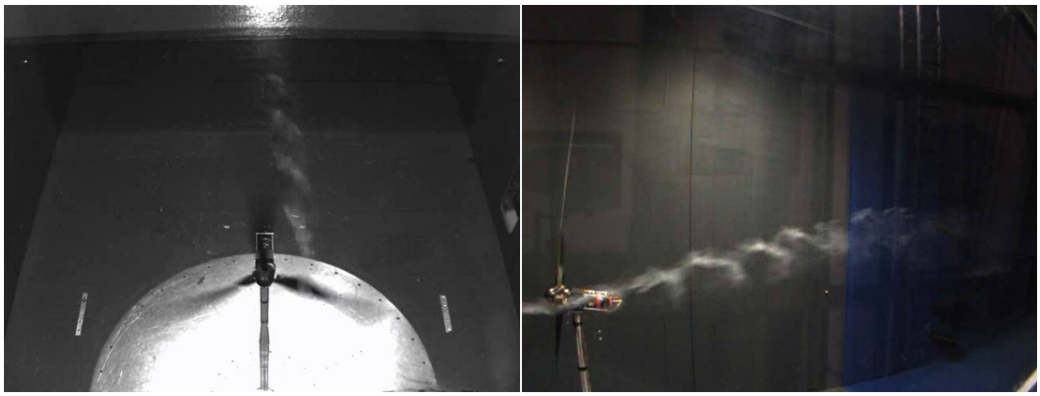

Figure 4.1: *Wind turbine operating in uniform flow in the high-speed and low-turbulence test section at Politecnico di Milano Wind tunnel. Wake visualization using smoke [3].*

Figure 4.2: *Wind turbine installation in the high-speed low-turbulence test section at Politecnico di Milano Wind Tunnel [3].*

A is the area of the wind turbine blades and S the wind tunnel test section area, while the wake blockage $A'/S = 0.21$ where A' is the area swept by the rotor. This causes has an influence on the forces acting on the wind turbine and on the wake that will be constrained in the test section boundary. The blockage effect has not been corrected on data measured on the turbine, to perform the comparison, since a direct comparison is possible between experimental and numerical results.

4.2.1 Domain geometry

The domain used for the calculation of the wind turbine loads extends 3 rotor diameters upstream and 13 downstream. The domain vertical height is 3.8m that is the height of the wind tunnel test chamber and the horizontal width is 4m. The mesh is structured with 640 points in the longitudinal direction, 80 in the lateral direction and 76 in the vertical. The rotor is described by 40 points along the diameter and approximately 1200 points over the rotor area.

Boundary conditions are imposed on the external boundaries of the domain: the air speed and direction is imposed at the inlet boundary, while Neumann boundary condition is imposed at the outlet. The sides of the domain are modeled as no-slip walls, since the reproduction of the wall boundary layer is not a fundamental issue in this study and would increase significantly the computational cost.

The wind turbine parameters has been modeled with the actuator line approach reported in section 2.1. The wind turbine geometrical data are introduced using the design parameters of the turbine and the aerodynamic characteristics of the blades realized by the group that realized the wind turbine experimental model (Bottasso et al. [3]). The aerodynamic characteristics of the blade airfoils have not been extracted from the design profiles, but have been identified with dedicated wind tunnel tests, as reported in Capponi [6].

4.2.2 Numerical setup

The computations have been conducted on CILEA [11] cluster[1]. The domain has been decomposed in 32 sub-domains in order to split the calculation between several CPUs: the average load per CPU is 114000 cells, that is close to the optimum load per CPU for the optimization of calculation time. A PISO (Pressure Implicit with Splitting of Operators) method is used. The methods used to solve the pressure and velocity equations are:

- pressure uses a conjugate gradient solver, with a diagonal incomplete-Cholesky preconditioner;
- velocity uses a bi-conjugate gradient solver, with a diagonal incomplete-LU preconditioner;

The numerical discretization schemes used for the calculation are:

- time discretization scheme is second order implicit;

[1] For this calculation up to 1200 CPUs were used, on 100 nodes, each equipped with 2 Intel $X5660$ hexacore processors and 24 Gb RAM, interconnected with Infiniband QDR Voltaire. A total of 5 Tb of MSA1500 disk space has been used. Post processing has been done on a DL980 node with 8way-512Gb RAM. The whole system is provided by Hewlett-Packard.

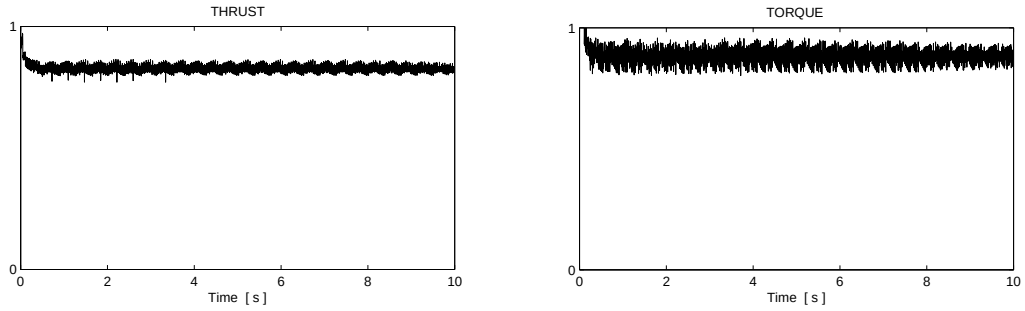

Figure 4.3: *Wind turbine thrust (left) and torque (right) time histories calculated with a uniform flow.*

- gradient discretization scheme is second order;
- divergence discretization scheme is second order;
- laplacian discretization scheme is second order, unbounded, conservative;

The time-step used for the calculation is 0.001 seconds, with a mean Courant number $C_{mean} = 0.03$ and a maximum $C_{max} = 0.21$, having a maximum angular rotation of the rotor each time-step of $\theta_B = 2.4^\circ$, that means around 150 time-steps to make a complete rotation. In these conditions the tip of the blades stay in a cell for 2 time steps.

4.3 Power generation

The analysis on the performances of the wind turbine are separated in two distinct sections: in section 4.3.1 the calculated force time histories and some analysis on the spectra are reported, while in section 4.3.2 the performances of the wind turbine at different Tip Speed Ratio (TSR) and blade pitch angle (θ_P) are reported. All the results are presented in non-dimensional form, in particular the frequencies are proposed as f/f_T, being f the frequency and $f_T = \omega/2\pi$ the fundamental turbine rotation.

4.3.1 Wind Turbine loading time history

LES calculations start with an initialized flow field, which needs to reach a stable operating condition. In Figure 4.3 a typical example of the thrust and torque time history during a calculation is reported. It is possible to recognize the initial transitory until reaching a stable operation after around a second (1000 time-steps) of calculation. The solution remains stable for the entire duration of the calculation.

The results for a particular configuration of TSR and blade pitch angle are reported in Figure 4.6. In all signals it is possible to see that it is not constant. The first chart reports the blade area as a function of time: this should be a line across the graph, but it is not the case. The blade area is computed each time step, as reported in section 2.2.2, summing the contribution in each cell given by the length l of the segment of actuator line that crosses the cell and the local chord $c(r)$ at the mid of the segment. The structured grid leads to a calculation of the actuator line forces that are changing every time-step: this leads to a signal that has a maximum variation of blade area $\Delta S_{MAX} = \pm 2.3\%$ and a standard deviation $\sigma_S = 0.1\%$. The line forces calculated at different locations on the blade can be seen in Figure 4.4.

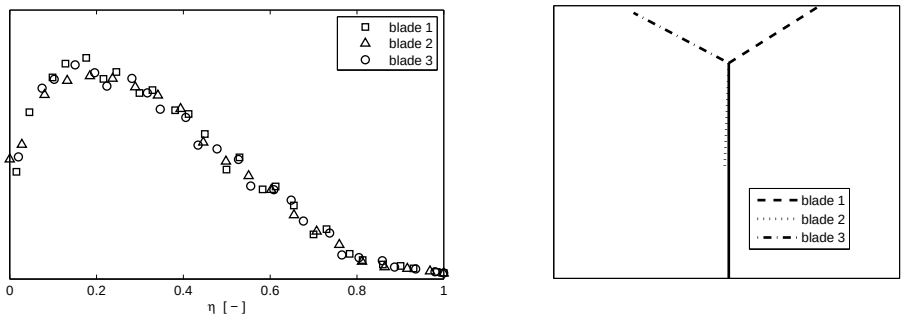

Figure 4.4: *Instantaneous axial load on the turbine blades (left) and position of the rotor (right).* $\eta = 0$ *is the blade tip,* $\eta = 1$ *is the blade root.*

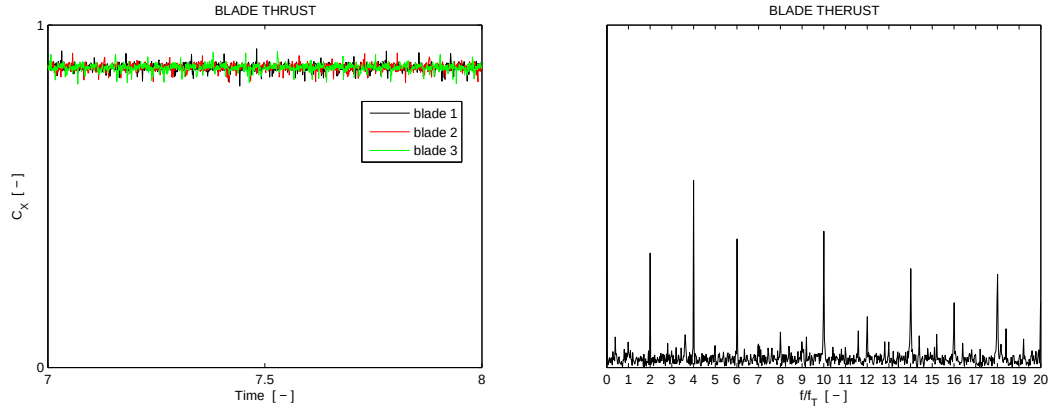

Figure 4.5: *Blade thrust time history (left) and spectrum (right) for uniform flow.*

The force time histories for each blade are reported in Figure 4.5. The axial forces show very low fluctuations around the mean value, the spectrum shows a peak at $2f_T$ and $4f_T$: this can be ascribed to the procedure used to calculate the blade area. The actuator line performances are calculated on a cartesian grid: this means that there are some frequencies that are due to the passage of the blade across the grid. The fundamental rotation f_T is noticeable with a low amplitude, while the $2f_T$ and the $4f_T$ are more evident since the path followed by the line on the grid presents a symmetry around the horizontal line and the vertical line that cross the axis position. The total blade area signal presents the characteristic frequencies reported in Figure 4.6: several peaks are visible in the graph, in particular the frequency corresponding at $6f_T$ (that is the sum of the $2f_T$ of the blades reported in Figure 4.5, since the three contributions are 120° out of phase).

The thrust time history shows small oscillations around the mean value. Very evident is again the $6f_T$, but it can be mainly imputed to the calculation of the blade area, while it can be seen the contribution of the $3f_T$ that is the blade passage and all his multiples. On axial force is possible to note a frequency content that is a multiple of $0.4f_T$ and that has no feedback in the data analyzed: the explanation can be achieved looking in Figure 4.7 at the lateral forces acting on the turbine tower. Something similar to

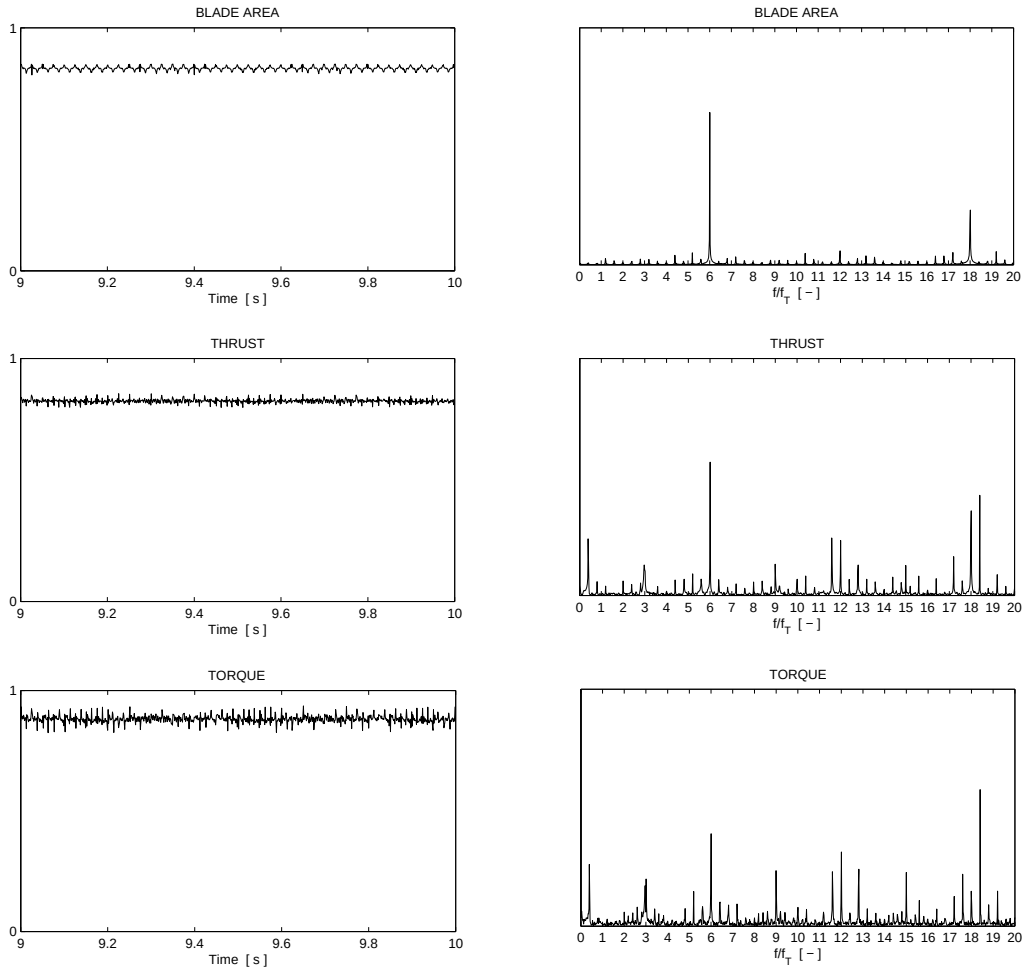

Figure 4.6: *Calulated blade area (top), wind turbine thrust (center) and torque (bottom) time histories (left) and spectra (right).*

vortex shedding occurs on the pylon: the spectrum amplitude shows the blade passage frequency $3f_T$ but also the $0.4f_T$ that can be identified also in the time history. This frequency at the contrary is hardly noticeable in the along-wind component of the tower force, where the $3f/f_T$ frequency is dominant. This result affects as already seen the thrust, where are clearly visible also the multiples of the $0.4f_T$, and is observable also in the torque signal though only the first frequency is evident while the multiples are muted. Torque shows clear peaks in correspondence of the multiples of the blade passage frequency $3f_T$.

An interesting result that can be achieved with the features of this solver can be seen in Figure 4.8 where the time-histories of thrust and power coefficient are reported: the simulation is carried on with a constant uniform inflow and a given blade pitch angle. After 10 seconds of simulation the blade pitch is instantaneously changed and the calculation is continued. The effective velocity model is able to reproduce the transient force that is obtained with a change in the wind turbine setting: it can be affirmed that the initial variation in the thrust and torque due to the non-initialized flow field, but the transient variation until reaching the regime condition that can be observed right

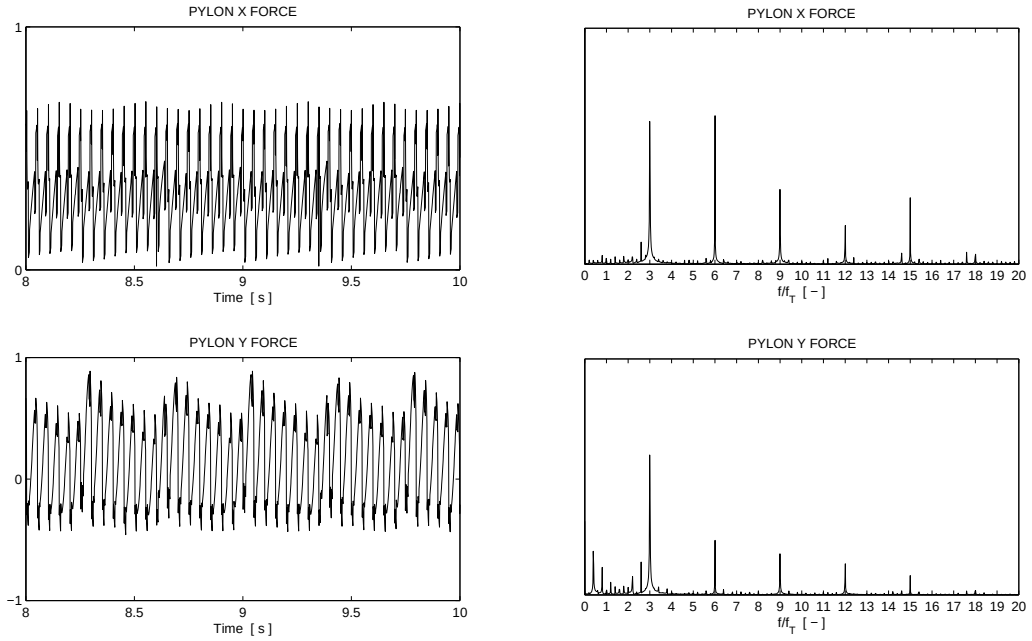

Figure 4.7: *Clculated axial force (top) and transversal force (bottom) time histories (left) and spectra (right).*

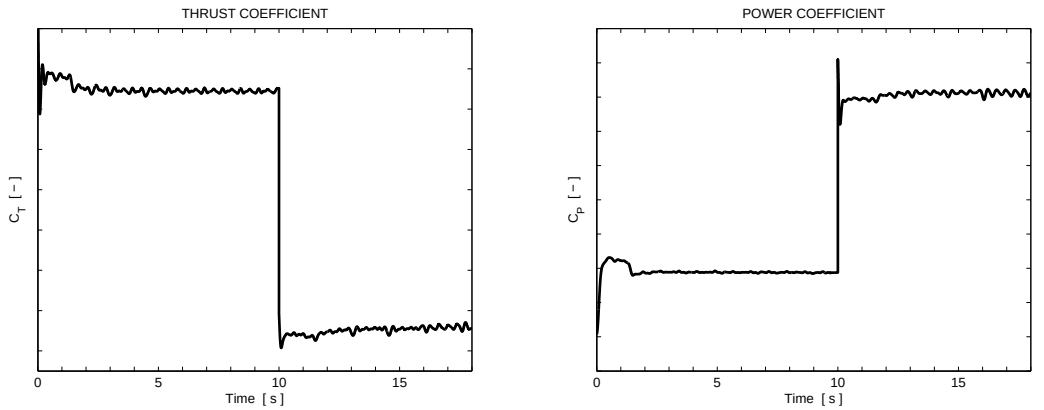

Figure 4.8: *Thrust and Power coefficient time history at fixed TSR. After* 10 *seconds the blade pitch is changed.*

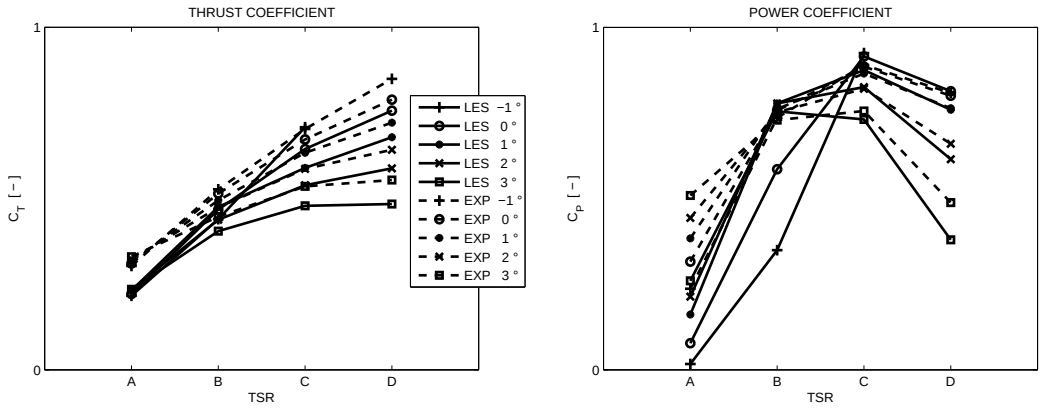

Figure 4.9: *Thrust and Power coefficients for different pitch angles generated by the wind turbine as a function of TSR.*

after the 10 seconds mark shows the reproduction of a transient solution. This feature of the model suggests that the wind turbine response to unsteady flow or changes of configuration due to the control system can be reproduced. In the future wind tunnel tests will be carried out to verify the quality of this result.

4.3.2 Wind Turbine performance

The result are reported in terms of integral thrust and power generated by the turbine: they will be presented in non-dimensional form, due to the fact that the owner of the wind turbine asked to not diffuse the data. As can be observed in the graphs, tip speed ratio TSR has not been reported, but are mentioned $TSR = A,B,C,D$ where A is low and D is a high TSR.

Figure 4.9 shows the thrust and the power coefficients as a function of TSR and blade pitch angle. It is possible to note that the trend of the C_T curves is similar, the value has some differences for low TSR, in-fact at $TSR = A$ the thrust is largely underestimated and the same thing can be affirmed for the power coefficient C_P. For higher TSR values the numerical and experimental differences reduce until becoming very low. The same affirmation can be done for the blade pitch angle: higher pitch angles (that mean lower angles of attack) show a better agreement with experimental data. This fact can be imputed to the effective velocity model: the performance of the model is good for rather low local angles of attack of the blade, and shows some difficulties in accurately reproducing higher angles of attack, around the stalled condition. An evidence of this can be seen in Figure 4.9 especially looking at the power coefficient C_P for $TSR = B$: it is largely underestimated by LES calculations for low pitch angles ($\theta_B = -1,0$), while a small increase in the blade pitch angle ($\theta_B = 1,2,3$) brings the results very close to the experimental data. Of course this phenomenon must imputed to the effective velocity model: the induced angle of attack α' (see equation 2.18 and Figure 2.10) changes with the value of the incidence angle of attack and is very different if the profile is stalled. The same consideration can be done analyzing the thrust and power coefficients C_T and C_P as a function of the blade pitch angle θ_B reported in Figure 4.10. The LES and experimental results show similar shapes, as already seen for the $C_T - TSR$ and the

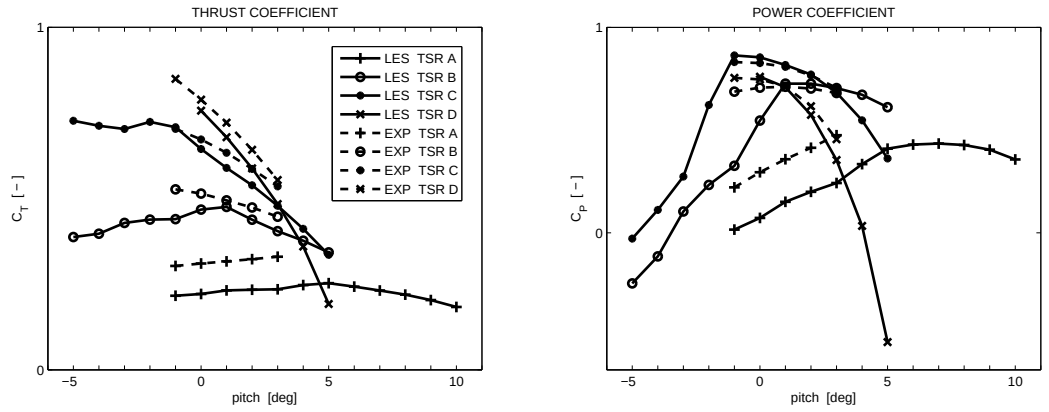

Figure 4.10: *Thrust and Power coefficients for different pitch angles generated by the wind turbine as a function of TSR.*

$C_P - TSR$ curves the agreement is better for high TSR ($TSR = C, D$) than for low TSR. An evidence of this can be seen for $TSR = B$: blade pitch angles higher than 1° show a satisfying agreement with experimental data, when the blade pitch becomes smaller than the "critical" angle the performances of the rotor have a sudden drop. This is clear especially looking at the $C_P - TSR$ curve for $TSR = B$ in Figure 4.10, but it is clear that also $TSR = C$ shows the same behavior.

4.4 Flow description

Large-Eddy Simulation allows to reproduce the large scales in the flow. In this case the incoming flow is uniform, there are no turbulent structures in the incoming flow; the only perturbations in the flow are generated by the presence of the wind turbine rotor, hub and tower modeled as actuator lines. In Figure 4.11 is shown an iso-vorticity surface and it is possible ti identify the turbulent structures in the wake of the wind turbine, like the tip and hub vortexes. In the same figure the position of the blades is reported as contour of volume force inserted in the domain. The actuator lines generate the tip and hub vortical structures that are driven downstream by the incoming flow. The tower itself produces a wake that is similar to what happens in the wind tunnel tests.This kind of measurements and visualizations are very difficult to do in full scale or in wind tunnel tests. Particularly interesting are the dynamics that involve the tip vortices that have been studied by Iungo [23] [21]. Tip vortexes are a typical vortical structure associated to the finite length of a wing, in our case it concerns a blade. At the tip of the wing the flow tends to move from the low-speed high-pressure side (the pressure side of the airfoil) to the high-speed low-pressure side (the suction side of the wing profile) moving externally of the wing; this generates a vortical structure that, for the wind turbine case, traces the path of the blade tips during the turbine operation. At the same time hub vortices develop from the blade root.

Looking in more detail at the wake measurements reported in Figure 4.12 it is possible to have more information about the performance of the wind turbine; the wake measurements for different non-dimensional distances x/D are reported. Experimental wake measurements are reported only for half rotor, while LES wake is traced all over

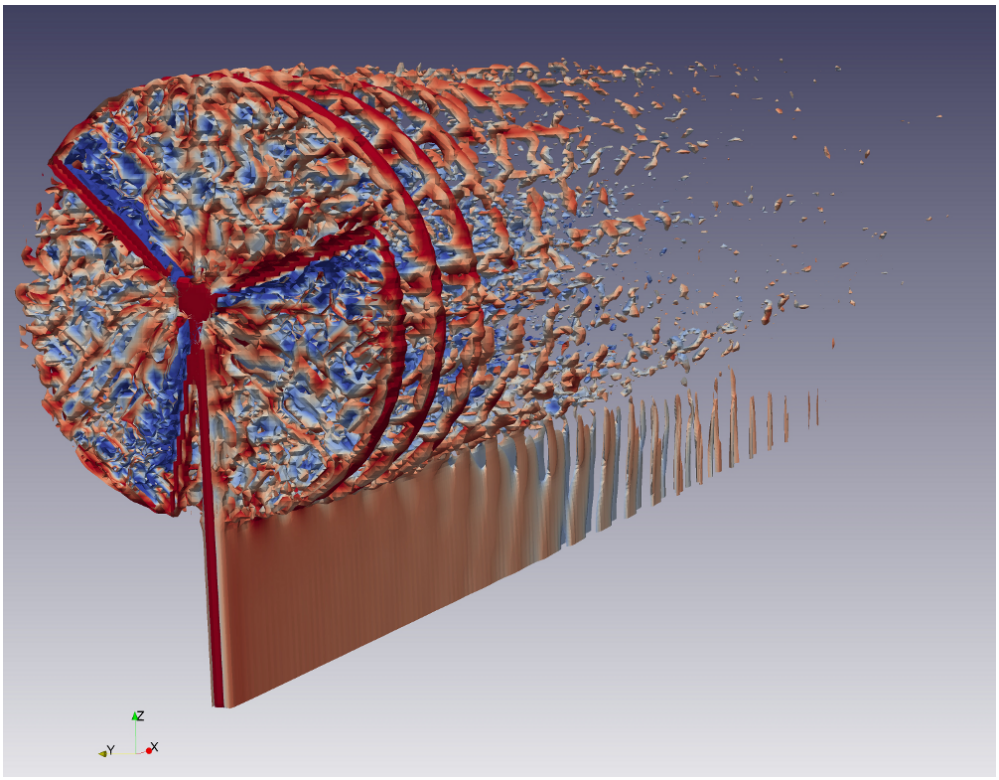

Figure 4.11: *LES of the wind turbine at $TSR = A$ in uniform flow. It is possible to identify the tip and hub vortexes, the vorticity produced by the pylon. The actuator lines are reported in order to show the position of the blades.*

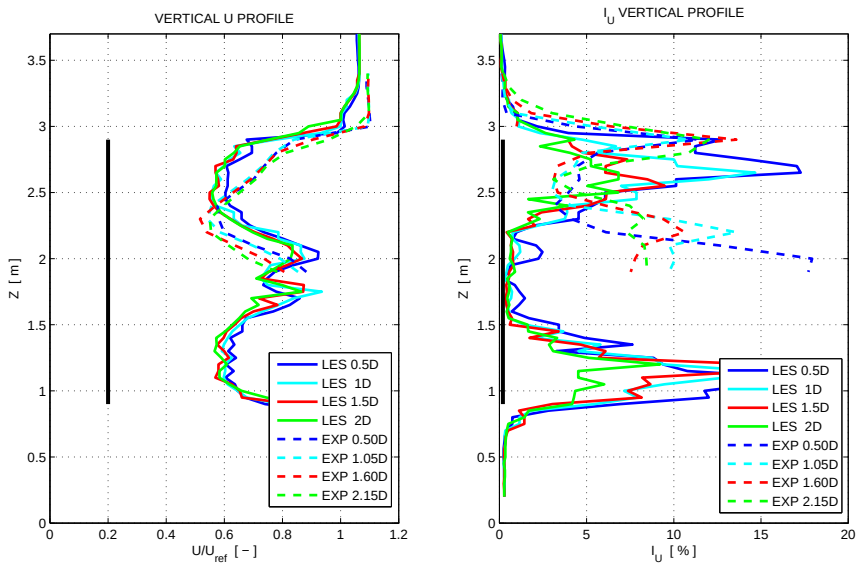

Figure 4.12: *Vertical profiles of axial wind and turbulence intensity in the wake of the wind turbine for experimental and LES calculations in uniform flow conditions at different x/D distances downstream of the rotor.*

the rotor.

The wake deficit makes evidence of the momentum transferred from the flow to the rotor: the figure shows that the integral thrust generated by the wind turbine is well reproduced with the LES simulation; nevertheless the distribution of the wake wind speeds shows some differences in the momentum subtraction. Experimental wake data show very low velocities close to the hub, while the wind velocities get higher near the tip of the blades. LES simulations on the contrary show higher wind speeds close to the hub and higher momentum deficit closer to the blade tip. This means that the forces are distributed differently on the blade: experimental forces seem to be higher close to the blade root than to the blade tip, while the LES blade loads, reported in Figure 4.4, show a higher load near the blade tip than on the blade root. The wake deficit information can be used to update the definition of the tabular aerodynamic characteristics of the blade sectional airfoils with the methodology proposed by Capponi [6].

LES calculations show a wake effect of the nacelle that is not similar to what is measured in the wind tunnel: this effect can be observed in the turbulence intensity profiles, where the flow seems very turbulent in the wind tunnel, while CFD simulations show a very smooth flow. Turbulence intensity in correspondence of the blade tips is well captured. An increase in turbulence intensity can be noticed in correspondence of the maximum wake momentum deficit, that means that experimental data show higher turbulence intensity close to the blade root and LES calculations near the blade tips.

Further analysis of the wind turbine wake is shown in Figure 4.13 where the non-dimensional vertical wind profiles of air speed and turbulence intensity in the wake of the wind turbine. The blockage effect of the rotor is clear, since the air speed out of the wind turbine wake is 10% higher than the incoming flow. The lower velocity value on the lower part of the profile is imputable to the presence of the tower, since the reported vertical profile crosses the center of the rotor. Analyzing a profile that is not shaded by the turbine pylon the wind speed is similar to the velocity in the upper side of the profile. As already seen for the wind profiles close to the rotor (see Figure 4.12), the profiles reported in Figure 4.13 show a very stable wake that starts the mixing in the central part at a non-dimensional distance $x/D = 5$ and starts to loose energy at $x/D = 8$. The high blockage that affects this test does not hides the wake expansion downstream the rotor that is visible for the distances of $x/D = 5$ and $x/D = 8$. Unfortunately the verification of this outcome cannot be done in the wind tunnel since the test section allows only a maximum distance of 2 rotor-diameter. Looking at the transversal velocity vertical profiles in Figure 4.13, some interesting considerations can be done: the lateral momentum on the vertical profile is generated by the angular momentum transferred to the rotor. The velocity profile has a different direction close to the hub and near the tip: this means that some sections of the blade concur at the production of power, while some others oppose. The angular momentum generated by the blades is transported at a considerable distance downstream of the turbine, showing a decrease after $x/D = 5$ and an almost complete reduction after $x/D = 8$. The vertical wind profile shows mean vertical velocities close to zero. Turbulence intensities reported in Figure 4.13 show large peaks located in correspondence of the blade tips, while, as already seen in Figure 4.12, the hub turbulence intensity peak is not visible. Turbulence diffuses after $x/D = 5$ for the along wind, the lateral and the vertical direction. In particular the turbulence intensity of the vertical component of the wind velocity points out the peaks in correspondence of

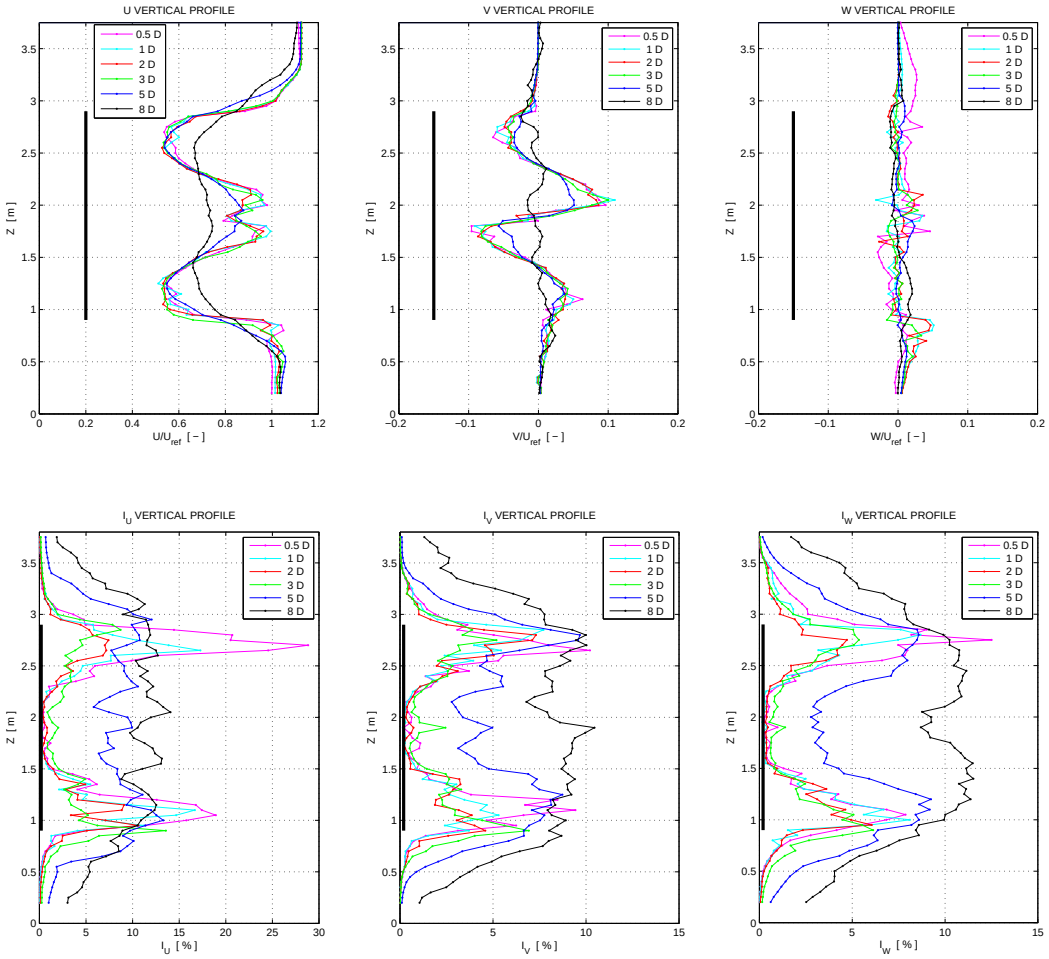

Figure 4.13: *Vertical profiles of wind velocity components (top) and turbulence intensity (bottom) in the wake of the wind turbine in uniform flow conditions at different x/D distances downstream of the rotor.*

the blade tips although the mean velocity is close to zero. The tip vortices give noticeable oscillations in the vertical flow component, contributing to the turbulence intensity.

Additional simulations have been conducted on a larger domain, extending 5 rotor diameters upstream and 15 downstream. The width and the height of the computational domain is 2.5 times larger and 2.5 times higher than the wind tunnel width and height. In this case the blockage of the rotor area reduces from a value of 0.21 to 0.03. The calculation us conducted using a grid size that is double of the one used for the previous calculation, and for this reason the LES filter has double the size.

Results are reported in Figure 4.14: the reference undisturbed wind speed is reached right outside the wind turbine wake, while for the wind tunnel blockage calculation the flow speed up reaches 10% of the reference wind speed V_∞. The reduction of the wind speed in correspondence of the wind turbine corresponds to an implicit increase of TSR, that for this configuration generates the same thrust coefficient and an increase of 10% in the power coefficient. The thrust coefficient depends on the axial wind deficit in the rotor wake: the shape of the vertical profiles of axial wind for high blockage are reported in Figure 4.13 while the wind profiles for low blockage are reported in Figure 4.14. Low blockage profiles show a different shape than wind tunnel profiles: flow velocity at hub height is lower than for the high blockage simulations, and the peak velocity deficit is lower than for the blocked condition. This could depend on the grid size that describes with less accuracy the hub. Lateral component of the wind in the wake shows a more regular path, suggesting that a more extended region of the blade contributes to the angular momentum to the rotor than for the simulation with high blockage: in fact the power coefficient shows an increase of 10%. Vertical wind profiles indicate that close to the wind turbine the flow on top of the wake has a positive component, that means that the air is going in the upward direction, since the flow is free to go around the obstruction offered by the rotor. Turbulence intensities are lower than for the high blockage simulation but this result is mainly affected by the filtering of the coarser grid. It is still possible to see the two peaks concentrated at the blade tips, but the contribution tends to diffuse more, since there is not the presence of the constraint of the wind tunnel walls.

The results of the Large Eddy Simulations in uniform flow gives some important informations: the main flow characteristics are well captured. Some discrepancies between experimental and wind tunnel measurement are noticeable and may be due to the assumptions that lie in the "effective velocity" model and to the tabular data used to describe the aerodynamic performances of the blade sections. Further improvements will be done in both the "effective velocity" model and the definition of the aerodynamic characteristics of the blades, in order to better match the experimental thrust and power data, and generate the correct wake deficit.

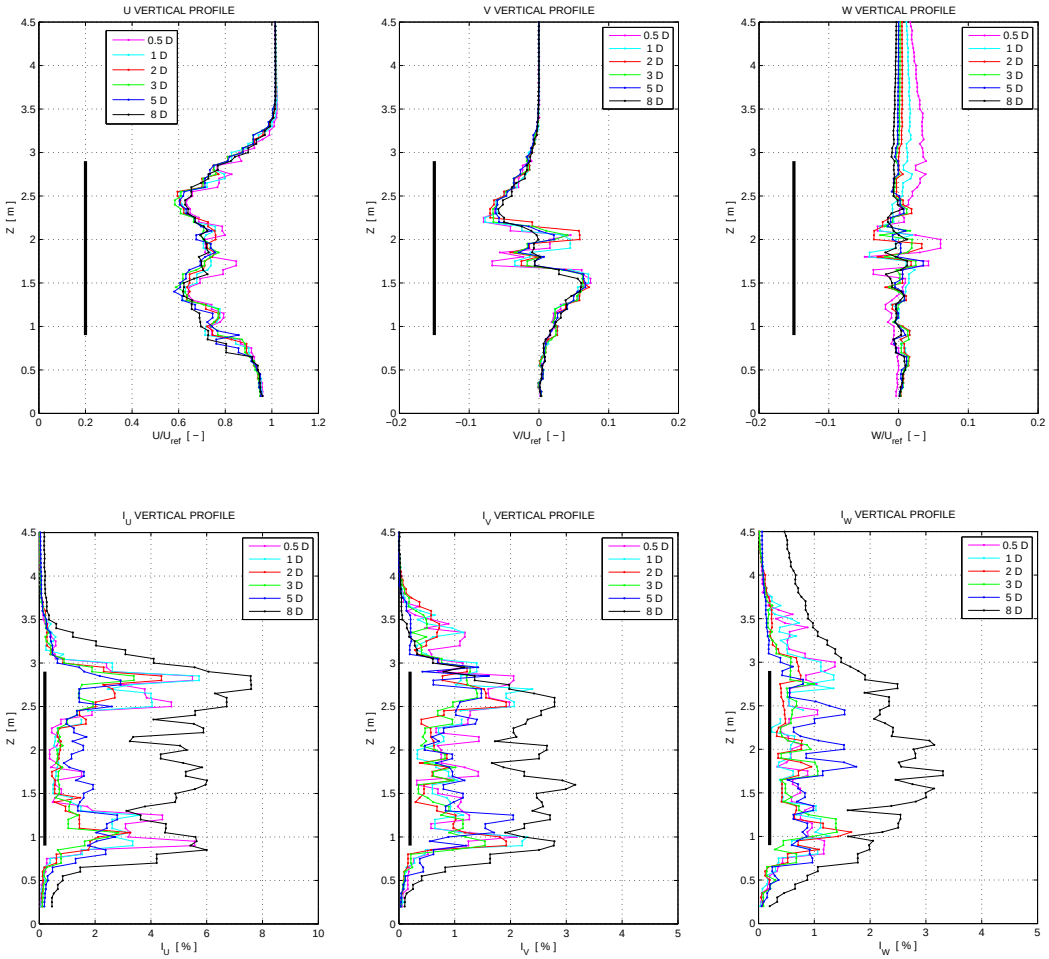

Figure 4.14: *Low blockage simulation. Vertical profiles of wind velocity components (top) and turbulence intensity (bottom) in the wake of the wind turbine in uniform flow conditions at different x/D distances downstream of the rotor.*

CHAPTER 5

Wind Turbine in turbulent flow

TURBULENT BOUNDARY LAYER Large Eddy simulations of the actuator line modeling of the wind turbine realized by prof. Bottasso [3] is presented. The turbulent inflow and the geometry of the domain reproduce the boundary layer test section of the Politecnico di Milano Wind Tunnel. The experimental data are only preliminary experimental results, since this is an ongoing activity and an extensive measurement campaign has been planned for the next years.

5.1 Wind Tunnel setup

The wind tunnel setup can be seen in Figure 5.1: the turbulent boundary layer flow is obtained with the spires placed at the beginning of the wind tunnel test section; on the ground the roughness elements are placed in order to get the desired mean wind profile, with the correct turbulence intensity and length scale. It is to note that an artificial trick was used to get the desired wind profile: the fans on the lower part of the wind tunnel are fed with less power than the one on the higher part. The wind turbine stands at a distance of 20 meters from the spires, 1 meter from the test section center-line. In the foreground there is the one-dimensional traversing system, consisting of a 4 meter long mast, that can be positioned either in the horizontal or in the vertical direction, equipped with 4 TFI[1] cobra probes. Several vertical and horizontal wind profiles have been measured in order to have a characterization of the wind turbine wake.

[1] Turbulent Flow Instrumentation Pty Ltd. – www.turbulentflow.com.au

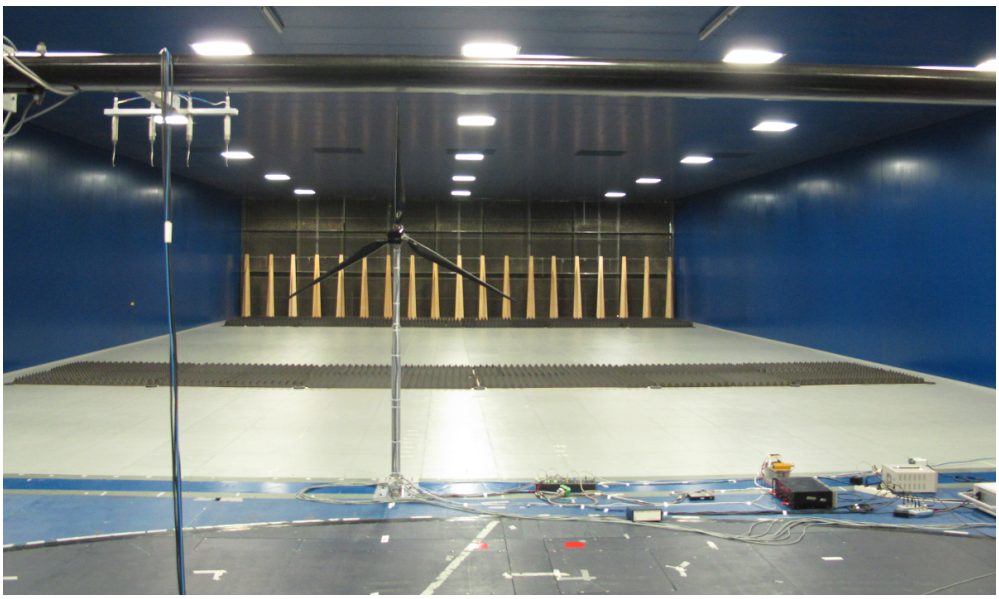

Figure 5.1: *Image of the experimental setup for wind tunnel wake measurements on the wind turbine. It is possible to identify the spires, the floor roughness. Close up are visible the cobra probes used for the measurement of the velocity in the wake of the wind turbine.*

5.2 Numerical setup

The numerical setup is similar to what has been done for the uniform flow. In this case the lateral and the upper and lower walls have been modeled as no-slip walls, in order to consistently reproduce the wind tunnel flow field and the boundary layer on the walls. The computational grid consists of 16.7 millions cells. Part of them (2.3 millions) are tetrahedral cells used to describe the volume close to the spires while the rest is described by parallelepipeds. The domain extents 10 meters upstream of the spires, and 50 meters downstream, the lateral size is 14 meters and the height is 3.8 meters, reproducing accurately the size of the boundary layer test section. The size of the mesh in the location of the wind turbine and in the wake is the same as the one used for the calculation in Rocchi et al. [46] and presented in section 4.2.1 for the uniform flow calculations.

The wind velocity turbulent boundary layer profile is reported in Figure 5.2 and shows a good agreement between the preliminary experimental results and the LES calculations. The non uniform power given to the fans that drive the flow in the testing chamber reported in section 5.1 may justify the slightly difference in the profile's slope and the slightly different shape on the higher part. The along wind turbulence intensity is reproduced with good accuracy by LES simulations, although the relation reported in equation 3.2 is not exactly fulfilled.

5.3 Power generation

The performances of the wind turbine operating in turbulent flow are reported in terms of integral thrust and power generated by the wind turbine. The report for the turbine loads will again be split in the analysis of the force time histories and successively

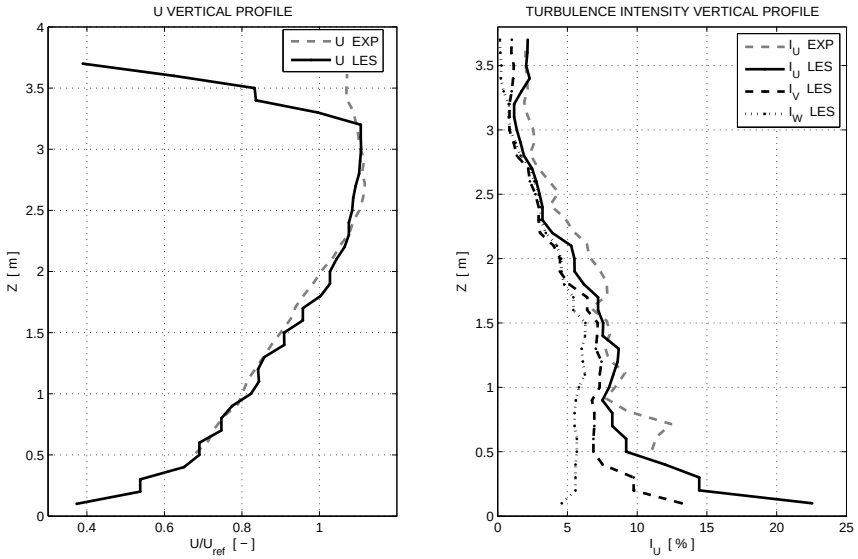

Figure 5.2: *Mean wind and turbulence intensity vertical profiles at the rotor location.*

analyze the performances.

5.3.1 Wind Turbine loading time history

In Figure 5.3 are reported the results for a specific TSR and blade pitch angle. Differently from what has been seen in section 4.3.1 and shown in Figure 4.6 for the uniform flow condition, turbulence has a noticeable effect on thrust and torque time histories. Thrust and torque present large fluctuations around the mean value, mainly due to the interaction with the turbulence structures. The $3f_T$ blade passage frequency can be clearly identified in both the thrust and the torque spectrum: the power of the signal is spread over a wide band of frequencies around the multiples of the blade passage frequency; on the contrary for the uniform flow the power of the signal is limited to a frequency very close to the blade passage frequency multiples. On the tower the unsteady lateral force is not so evident as in the uniform flow conditions, and the $3f_T$ blade passage frequency is highlighted. The analysis on thrust generated on each blade can be seen in Figure 5.4: the time history shows that the forces have large fluctuations since the blades rotate in the turbulent boundary layer changing the axial wind speed with the height. The three signals are 120° out of phase, since the rotor consist of three blades. Comparing this signal with the blade thrust time-histories presented in Figure 4.5 is is possible to observe the much larger fluctuations in the blade thrust coefficient C_X for the turbulent flow simulations than for the uniform flow. Figure 5.5 is reported the spectrum of the blade thrust force: compared to Figure 4.5 the fundamental rotation f_T is the dominant frequency. The numerical $2f_T$ frequency is still visible, but the fundamental rotation of the blade in the boundary layer has the largest influence on the spectrum.

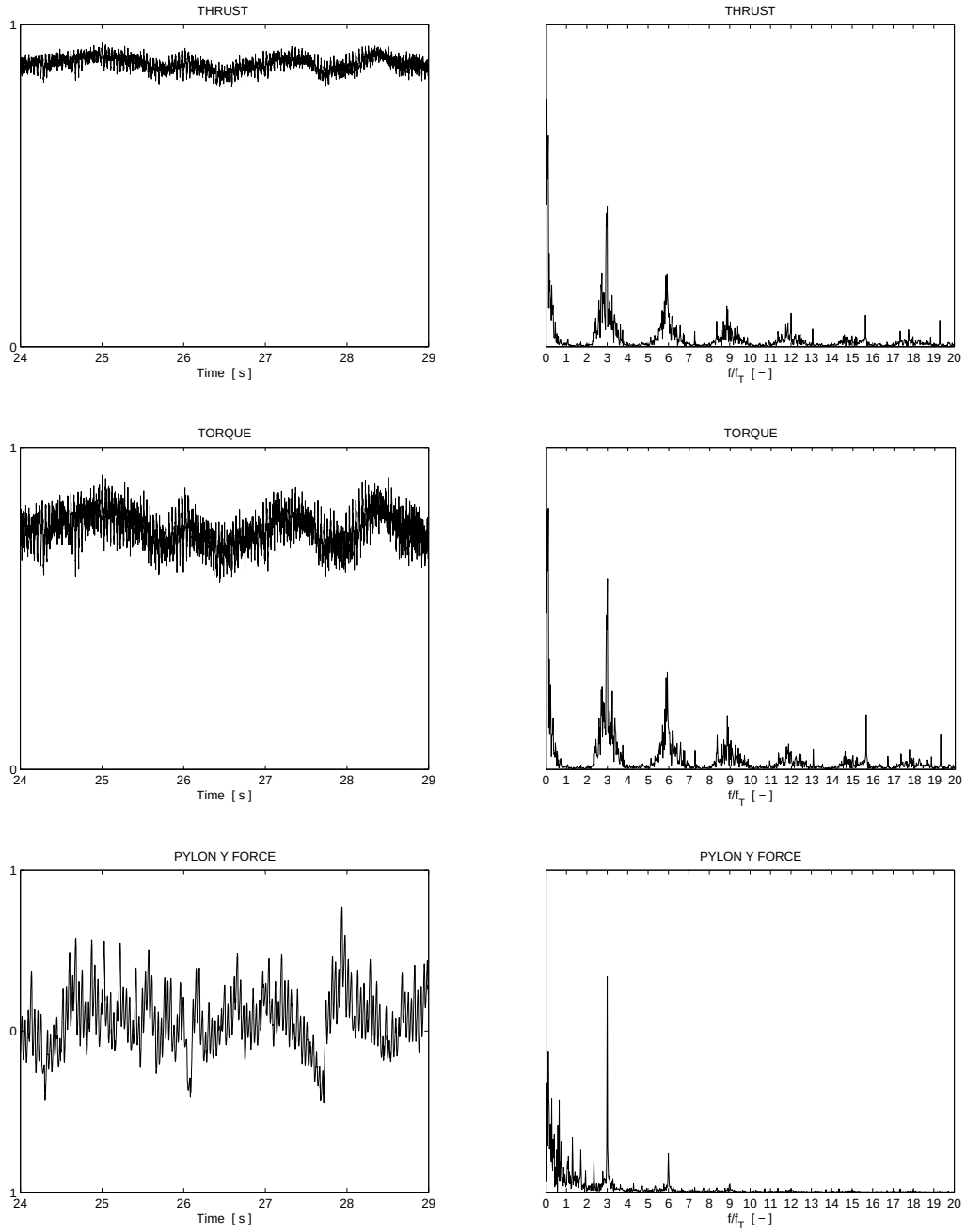

Figure 5.3: *Thrust (top), torque (center) and lateral force on the tower (bottom) time histories (left) and spectra (right) for a given TSR and blade pitch angle in turbulent flow.*

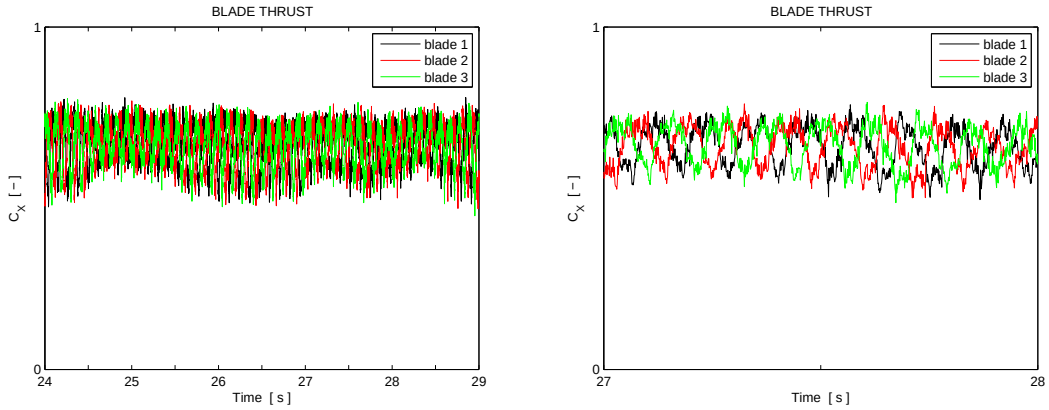

Figure 5.4: *Blade thrust time histories on each blade in turbulent wind condition.*

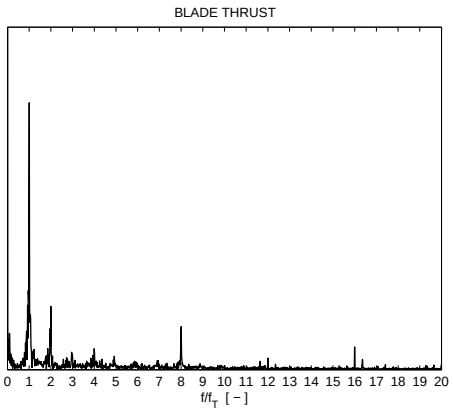

Figure 5.5: *Blade thrust spectrum for the simulations in turbulent wind.*

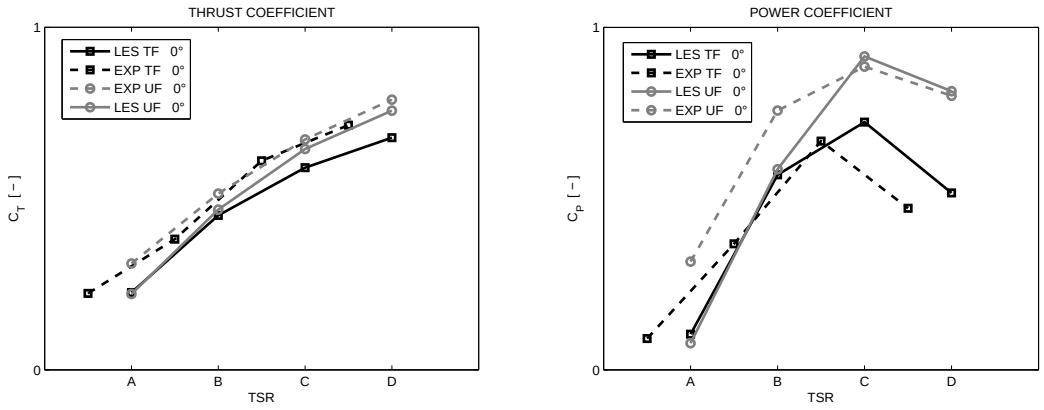

Figure 5.6: *Thrust and power coefficients for the wind turbine in uniform (UF) and turbulent (TF) flow conditions at a constant blade pitch angle.*

5.3.2 Wind Turbine performance

The mean thrust and power coefficient of the wind turbine working in different flows and at different TSR can be observed in Figure 5.6. Experimental thrust coefficient does not changes too much from the uniform to the turbulent flow condition: mean thrust seems not to be influenced by turbulence, but in this case the blockage effect of the wind tunnel has not been evaluated and corrected. On the contrary power coefficient shows a dependence on the turbulence effect: uniform flow presents higher power coefficient, especially for high TSR values, and the same result is achieved by LES simulations.

5.4 Flow description

The flow that is obtained in a turbulent boundary layer flow for the $TSR = C$ is reported in Figure 5.7. It is possible to see the rapid decay of the wake structures and the turbulent mixing of the wake. Just in front of the wind turbine it is possible to see the slow down of the flow due to the thrust on the turbine that is acting on the incoming flow.

Looking with more detail to the wake velocities reported in the Figures 5.8, 5.9, 5.10, 5.11, it is possible to make some comments on the results reported in Figures 5.6: as already mentioned in section 4.4, the axial wake deficit gives an indication on the wind turbine thrust, while the vertical profile of transversal velocity shows the torque generated on the rotor.

Moving through the figures, it is possible to see that changing TSR the wake profile changes largely: for $TSR = A$ the maximum axial flow reduction is close to $0.6U/U_{ref}$ while for $TSR = D$ the lowest wake velocity is lower than $0.3U/U_{ref}$. The mixing of the flow due to turbulence is so high that the wake starts fading out after 2 rotor-diameters, while the uniform turbulence case the wake structure breaks up after $5D$.

A similar effect can be seen looking at the wake vertical profiles of transversal velocity. Maximum power generation is obtained for $TSR = C$, and this can be verified looking to the maximum flow rotation that is reached at a certain distance from the hub: the angular momentum that is transferred to the rotor is maximum. The rotation of the wake is higher for $TSR = B$, but the maximum transversal velocity is obtained closer

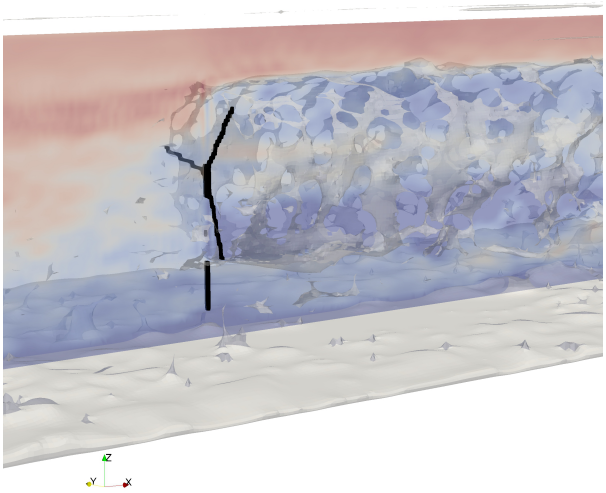

Figure 5.7: *Turbulent flow visualization for $TSR = C$. The wind turbine is identified by the black area representing the location where the forces are inserted on the grid. The image reports the along wind component of vorticity magnitude (colored in gray) and the wind tunnel vertical center-plane colored by velocity magnitude.*

to the hub.

Turbulence intensity in the wind turbine blade shows a high dependence on TSR at which the wind turbine is working. For $TSR = A$, a low value of Tip Speed Ratio, the turbulence intensity shows a minor increase in the longitudinal direction, more evident in the lateral and vertical direction. Turbulence intensity at in correspondence of the blade tips is higher than in the wind turbine wake. Increasing the TSR all values of turbulence intensity increase, the most evident is the along wind turbulence intensity that at $TSR = D$ in correspondence of the top of the rotor becomes 4 times higher than the turbulence intensity at $TSR = A$.

It is evident that $TSR = A$ represents the situation of a strong wind, where the wind turbine power is not harvesting the maximum power from the wind: the wake deficit is not very big and the turbulence intensity in the wake is increased, but not significantly. Increasing the rotational speed of the rotor, let's say a typical working point is $TSR = C$, the wake deficit becomes important, and the turbulence intensity increases largely. This regime is used for low speeds and extracting the maximum energy from the wind. It is evident that the power generation in a wind farm will not be significantly affected in case of strong winds, while in light winds the wind farm performances will be noticeably affected if the direction of the wind drive the wakes of the upwind wind turbines on the following rows. The effect will not be only visible on the thrust and power generated by the wind turbines but will affect also the loads on the blades and on all the components that may suffer fatigue damages due to the increase in the turbulence intensity in the flow.

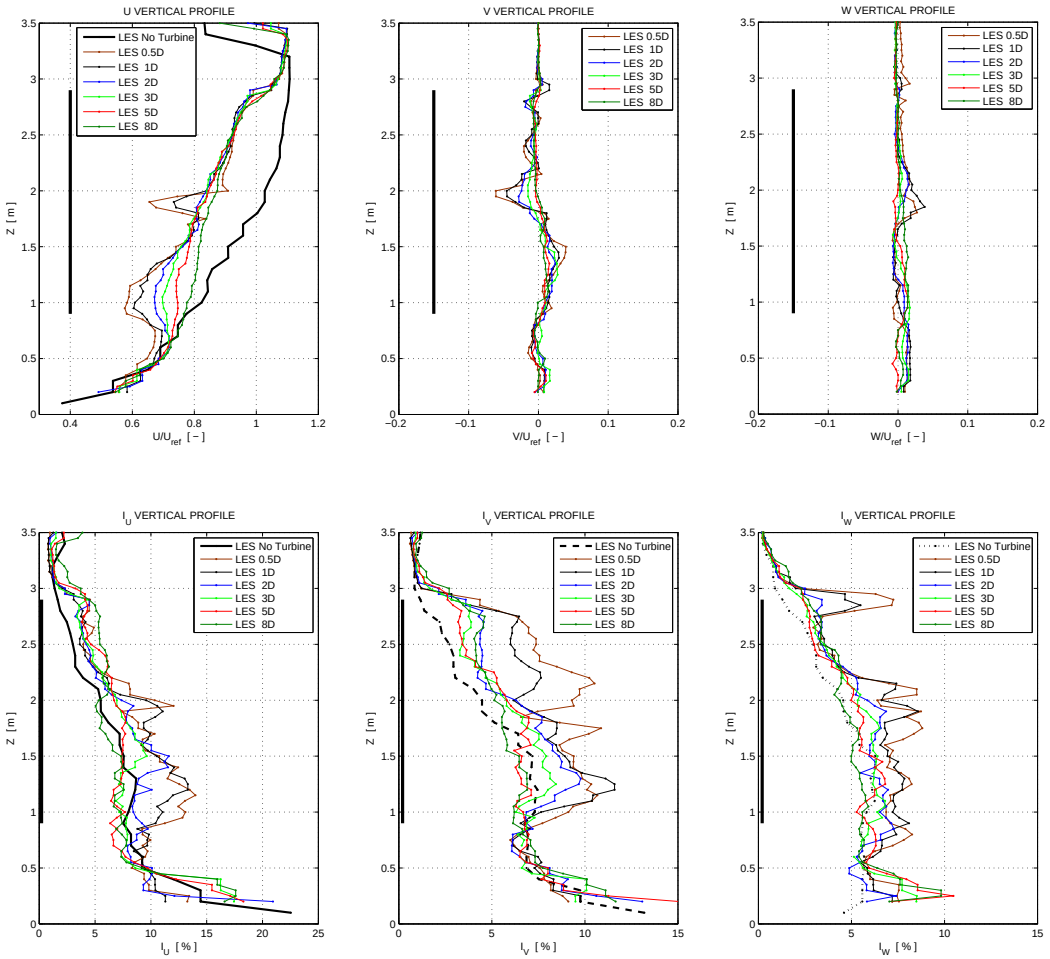

Figure 5.8: *LES Vertical profiles of wind velocity (top) and turbulence intensity (bottom) in the wake of the wind turbine operating at $TSR = A$ in turbulent flow conditions at different x/D distances downstream of the rotor.*

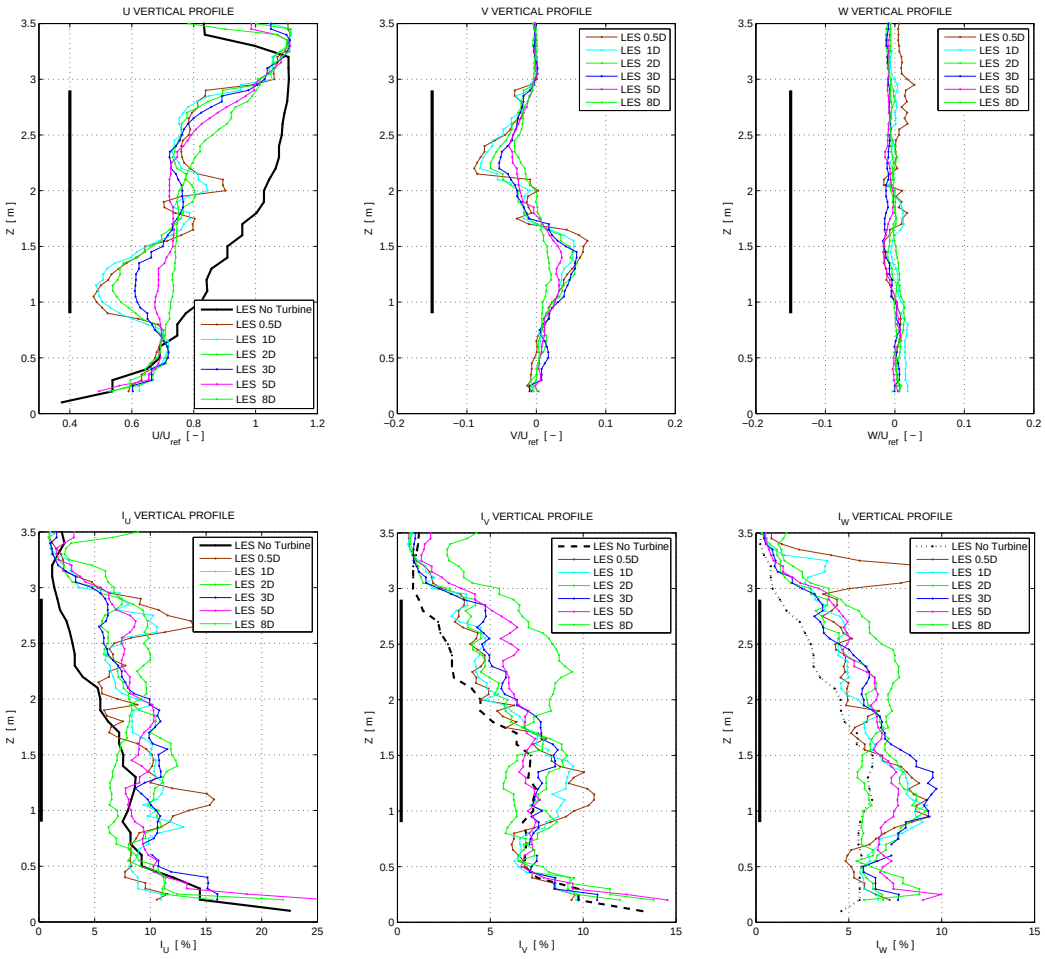

Figure 5.9: *LES Vertical profiles of wind velocity (top) and turbulence intensity (bottom) in the wake of the wind turbine operating at $TSR = B$ in turbulent flow conditions at different x/D distances downstream of the rotor.*

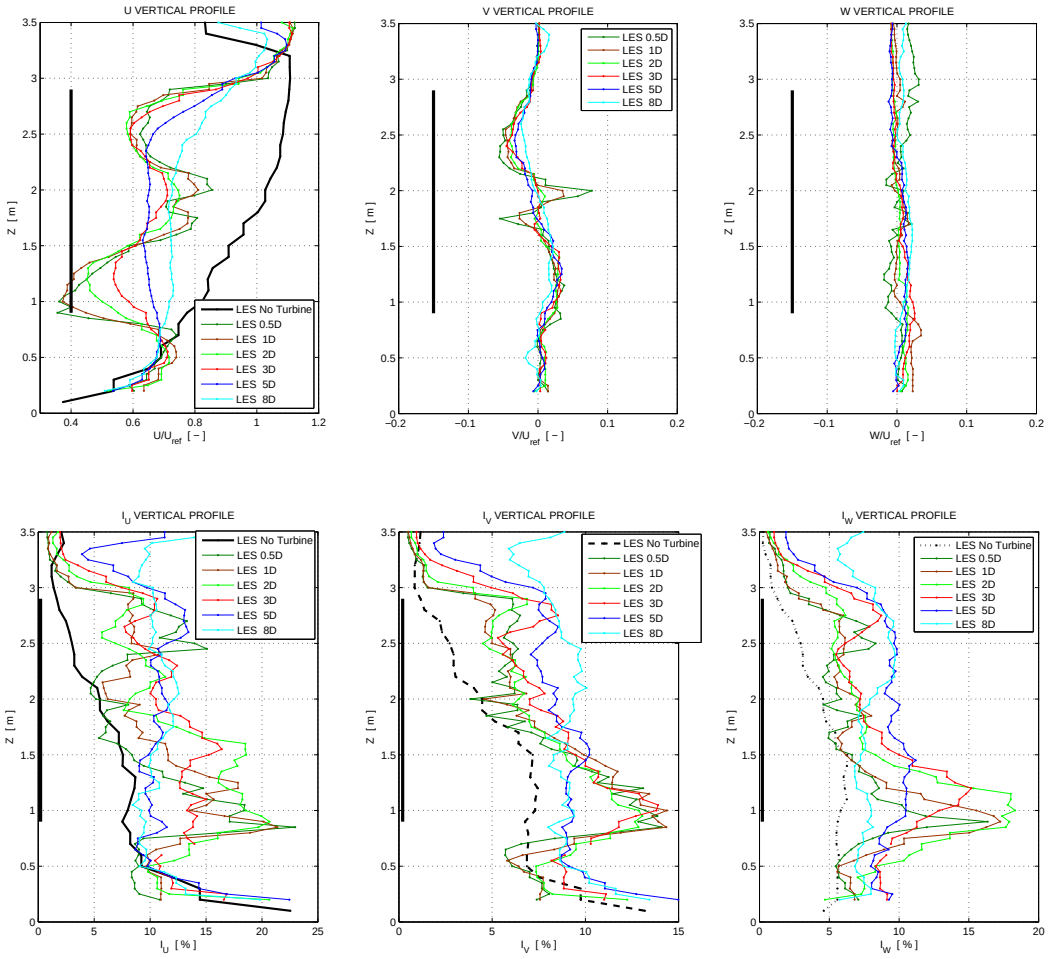

Figure 5.10: *LES Vertical profiles of wind velocity (top) and turbulence intensity (bottom) in the wake of the wind turbine operating at $TSR = C$ in turbulent flow conditions at different x/D distances downstream of the rotor.*

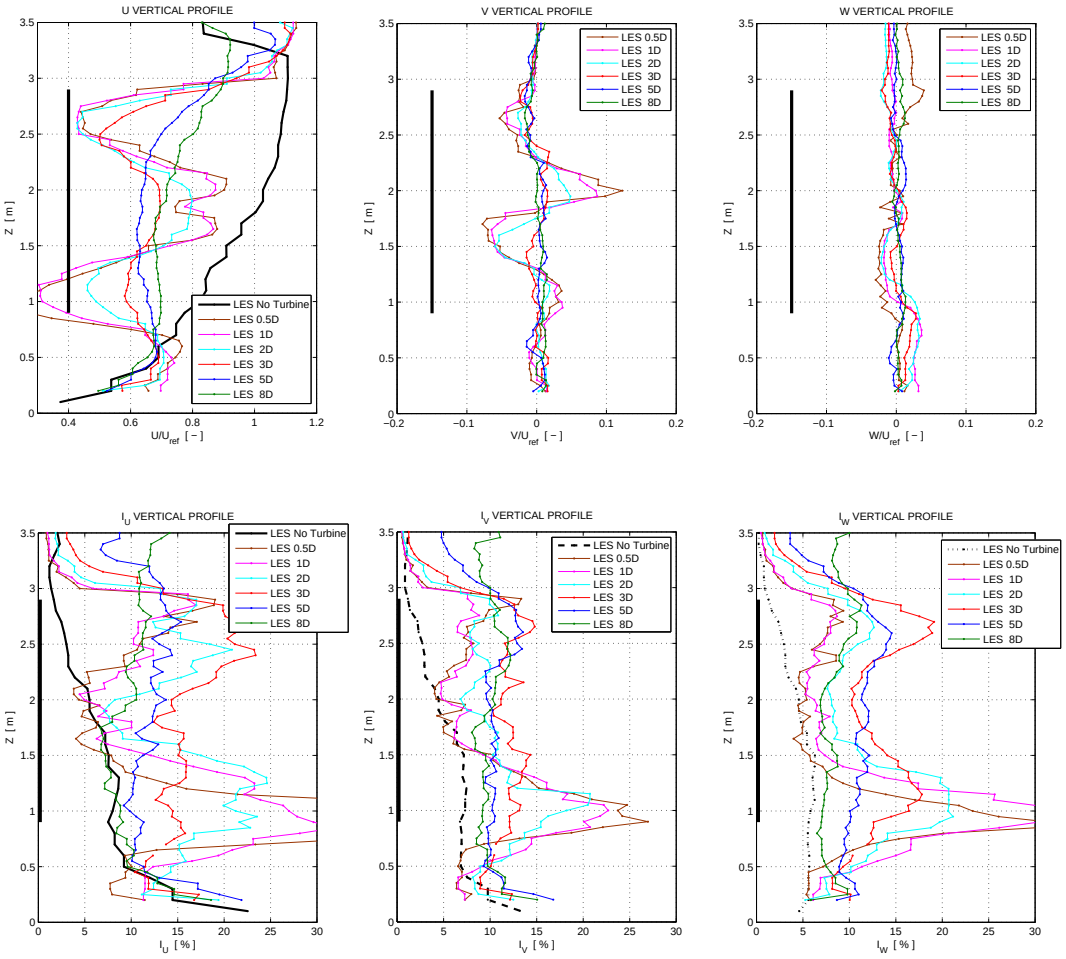

Figure 5.11: *LES Vertical profiles of wind velocity (top) and turbulence intensity (bottom) in the wake of the wind turbine operating at $TSR = D$ in turbulent flow conditions at different x/D distances downstream of the rotor.*

Conclusion

This work presents a new model for the calculation of the wind turbine loads and the reproduction of the flow field around a wind turbine in turbulent flow using a Large Eddy Simulation approach implemented in the open-source OpenFOAM environment. A new model called "effective velocity" model is proposed as an alternate solution to classical BEM methods to calculate the wind turbine loads using an actuator line approach.

LES calculations are conducted for uniform flow and turbulent boundary layer flow conditions. The numerical simulation results in uniform flow are compared with experimental wind tunnel data and the agreement between them is satisfying, especially when the blades are not working close to stalled condition. Wake wind profiles of mean axial velocity and turbulence intensity show the peculiar characteristics of the wake of a wind turbine.

The model presents the ability to reproduce the unsteady characteristics of the rotor operation in uniform flow and the performances in transient conditions.

Turbulent boundary layer simulations show a good agreement with preliminary wind tunnel tests. Wake wind profiles show that the wake structures break up closer to the wind turbine when the turbulence of the incoming wind is reproduced, but the momentum deficit in the wake extends several rotor-diameters downstream.

Future efforts must be dedicated to the identification of the aerodynamic of the blade aerodynamic tabular data used for the calculation of the loads on the rotor and to the development of the "effective velocity" model in order to correctly model all the blade working conditions.

Bibliography

[1] Bayati I.A. *Design and validation of a "hardware-in-the-loop" experimental rig for wind tunnel tests on offshore wind turbines*. Dipartimento di Ingegneria Meccanica – Politecnico di Milano – Milano – Italy, 2011. MSc Thesis.

[2] Blocken B., Stathopoulos T., Carmeliet J. Cfd simulation of the atmospheric boundary layer: wall function problems. *Atmospheric Environment*, 41(2):238–252, 2007.

[3] Bottasso C.L., Campagnolo F., Croce A., Maffenini L. *Development of a Wind Tunnel Model for Supporting Research on Aero-servo-elasticity and Control of Wind Turbines*. 13^{th} International Conference on Wind Engineering – Amsterdam, The Netherlands, 2011. Conference Proceedings.

[4] Burton T., Sharpe D., Jenkins N., Bossanyi E. *Wind Energy Handbook*. John Wiley & Sons, 2001.

[5] Cadei F. *Analisi RANS CFD di aerogeneratori in supporto al progetto ed alla sperimentazione in galleria del vento*. Dipartimento di Ingegneria Aerospaziale – Politecnico di Milano – Milano – Italy, 2011. MSc Thesis.

[6] Capponi M. *Analisi e miglioramento delle caratteristiche aerodinamiche di un modello di aerogeneratore per prove in galleria del vento*. Dipartimento di Ingegneria Aerospaziale – Politecnico di Milano – Milano – Italy, 2011. MSc Thesis.

[7] Cermak J.E., Arya S.P.S. Problems of atmospheric shear flows and their laboratory simulation. *Boundary-Layer Meteorology*, 1(1):40–60, 1970.

[8] Chamorro L.P., Porté-Agel F. A wind-tunnel investigation of wind-turbine wakes: Boundary-layer turbulence effects. *Boundary-Layer Meteorology*, 132(1):129–149, 2009.

[9] Chamorro L.P., Porté-Agel F. Effects of thermal stability and incoming boundary-layer flow characteristics on wind-turbine wakes: A wind-tunnel study. *Boundary-Layer Meteorology*, 136(1):515–533, 2010.

[10] Chamorro L.P., Porté-Agel F. *Flow characterization of wind-turbine wake(s) developed in a boundary layer flow with different thermal stratifications: A wind-tunnel study*. 5^{th} International Symposium on Computational Wind Engineering – Chapel Hill, North Carolina, 2010. Conference Proceedings.

[11] CILEA. *Consorzio Interuniversitario*. High Performance Computing. hpc.cilea.it.

[12] Davenport A.G. Rationale for determining design wind velocities. *Proceedings of the American Society of civil Engineers – Journal of the Structural Division*, 86:39–68, 1960.

[13] Diana G., De Ponte S., Falco M., Zasso A. A new large wind tunnel for civil-environmental and aeronautical applications. *Journal of Wind Engineering and Industrial Aerodynamics*, 74–76(1):553–565, 1998.

[14] Druault P., Lardeau S., Bonnet J.P., Coiffet F., Delville J., Lamballais E., Laergeau J.F., Perret L. Generation of three-dimensional turbulent inlet conditions for large-eddy simulation. *AIAA Journal*, 42(3):447–456, 2004.

[15] Dyrbye C., Hansen S.O. *Wind Loads on Structures*. John Wiley & Sons, Ltd, 1997.

[16] EWEA. *The European offshore wind industry key 2011 trends and statistics*. The European Wind Energy Association, January 2012. web site – www.ewea.org.

[17] Hansen M.O.L. *Aerodynamics of Wind Turbines*. Earthscan, 2008.

[18] IEC 61400. *Wind Turbines – Part 1: Design Requirements*. IEC 61400-1, 2001.

[19] Irwin H.P.A.H. The desing of spires for wind simulation. *Journal of Wind Engineering and Industrial Aerodynamics*, 7(3):361–366, 1981.

[20] Iungo G.V., Coëffé J., Zhang W., Markfort C., Porté-Agel F. *Wind tunnel study of multiple wake interactions in wind farm with different layouts*. European Geosciences Union General Assembly – Vienna, Austria, 2011. Conference Poster.

[21] Iungo G.V., Skinner P., Buresti G. Correction of wandering smoothing effects on static measurements of a wing-tip vortex. *Experiments in Fluids*, 46(3):435–452, 2009.

[22] Iungo G.V., Wu Y.T., Porté-Agel F. Field measurements of wind turbine wakes with lidars. *submitted to Wind Energy*, 2011.

[23] Iungo V. *Survey of the dynamics of wake vorticity structures and of their experimental evaluation*. Department of Aerospatial Engineering – Università degli Studi di Pisa – Pisa – Italy, 2007. PhD Thesis.

[24] Ivanell S. *Numerical Computations of Wind Turbine Wakes*. Department of Mechanics – Kungliga Tekniska Höskolan – Stockholm – Sweden, 2009. PhD Thesis.

[25] Jimenez A., Crespo A., Migoya E., Garcia J. Advances in large-eddy simulation of a wind turbine wake. *The Science of Making Torque from Wind – Journal of Physics: Conference Series*, 75:1–13, 2007.

[26] Kataoka H., Mizuno M. Numerical flow computation around aeroelastic 3d square cylinder using inflow turbulence. *Wind and Structures*, 5(2–4):379–392, 2002.

[27] Kondo K., Murakami S., Mochida A. Generation of velocity fluctuations for inflow boundary condition of les. *Journal of Wind Engineering and Industrial Aerodynamics*, 67:51–64, 1997.

[28] Kraichnan R.H. Diffusion by a random velocity field. *The Physics of Fluids*, 13(1):22–31, 1970.

[29] Leung D.Y.C., Yang Y. Wind energy development and its environmental impact: A review. *Renewable and Sustainable Energy Reviews*, 16(1):1031–1039, 2012.

[30] Li N., Balaras E., Piomelli U. Inflow conditions for large-eddy simulations of mixing layers. *Physics of Fluids*, 12(4):935–938, 2000.

[31] Lignarolo L., Gorlé C., Parente A., Benocci C. *Large eddy simulation of the atmospheric boundary layer using OpenFOAM*. 13^{th} International Conference on Wind Engineering – Amsterdam, The Netherlands, 2011. Conference Proceedings.

[32] Lund T.S., Wu X., Squires K.D. Generation of turbulent inflow data for spatially-developing boundary layer simulations. *Journal of Computational Physics*, 140:233–258, 1998.

[33] Mann J. The spatial structure of neutral atmospheric surface-layer turbulence. *Journal of Fluid Mechanics*, 273:141–168, 1994.

[34] Mann J. Wind field simulation. *Probabilistic Engineering Mechanics*, 13(4):269–282, 1998.

[35] Manwell J.F., McGowan J.G., Rogers A.L. *Wind Energy Explained – Theory, Design and Application*. Wiley, 2009.

[36] Mikkelsen R. *Actuator Disc Methods Applied to Wind Turbines*. Department of Mechanical Engineering – Technical University of Denmark – Lyngby – Denmark, 2003. PhD Thesis.

[37] Nelson V. *Wind Energy – Renewable Energy and the Environment*. CRC Press, 2009.

[38] Nozawa K., Tamura T. Large eddy simulation of the flow around a low-rise building immersed in a rough-wall turbulent boundary layer. *Journal of Wind Engineering and Industrial Aerodynamics*, 90:1151–1162, 2002.

[39] Nozawa K., Tamura T. Large eddy simulation of wind flows over large roughness elements. *Proceedings of EACWE4*, 1(176), 2005.

[40] OpenFOAM. *The open source CFD toolbox*. Version 1.7.1. www.openfoam.org.

[41] Porté-Agel F. A scale-dependent dynamic model for scalar transport in large-eddy simulations: of the atmospheric boundary layer. *Boundary Layer Meteorology*, 112(1):81–105, 2004.

[42] Porté-Agel F., Meneveau C., Parlange M.B. A scale-dependent dynamic model for large-eddy simulation: application to a neutral atmospheric boundary layer. *Journal of Fluid Mechanics*, 415:261–284, 2000.

[43] Porté-Agel F., Wu Y.T., Lu H., Conzemius R.J. Large-eddy simulation of atmospheric boundary layer flow through wind turbines and wind farms. *Journal of Wind Engineering and Industrial Aerodynamics*, 99:154–168, 2011.

[44] Richards P.J., Hoxey R.P. Appropriate boundary conditions for computational wind engineering models using the $k-\varepsilon$ turbulence model. *Journal of Wind Engineering and Industrial Aerodynamics*, 46 & 47:145–153, 1993.

[45] Rocchi D., Schito P., Zasso A. *Evaluation of unsteady pressure fluctuations on surfaces using CFD*. 5^{th} International Symposium on Computational Wind Engineering – Chapel Hill, North Carolina, 2010. Conference Proceedings.

[46] Rocchi D., Schito P., Zasso A. Investigation on the relation between incoming wind characteristics and surface pressure distribution. *Journal of Wind Engineering and Industrial Aerodynamics*, submitted to ICWE13 Special Issue, 2011.

[47] Schepers J.G., Snel H. *Model Experiments in Controlled conditions – Final Report*. The Energy Research Center of the Netherlands ECN, 2007. MEXICO.

[48] Schreck S. *IEA Wind Annex XX: HAWT Aerodynamics and Models from Wind Tunnel Measurements*. NREL / TP-500-43508, December 2008. Final Report.

[49] Shen W.Z., Hansen M.O.L., Sørensen J.N. Determination of the angles of attack on rotor blades. *Wind Energy*, 12(1):91–98, 2009.

[50] Shen W.Z., Mikkelsen R., Sørensen J.N. Tip loss corrections for wind turbine computations. *Wind Energy*, 8(4):457–475, 2008.

[51] Smirnov A., Shi S., Celik I. Random flow generation technique for large eddy simulations and particle-dynamics modeling. *Journal of Fluids Engineering*, 123(1):359–371, 2001.

[52] Snel H. *A short history of wind turbine aerodynamics, or: From Betz to Better*. The second conference on the Science of Making Torque from Wind – Lyngby, Denmark, 2007. Invited presentation – ECN-L–07-068.

[53] Sørensen J.N., Shen W.Z. Numerical modeling of wind turbine wakes. *Journal of Fluids Engineering*, 124(2):393–399, 2002.

[54] Stull R.B. *An Introduction to Boundary Layer Meteorology*. Springer, 2009.

[55] Thomsen K., Sørensen P. Fatigue loads for wind turbines operating in wakes. *Journal of Wind Engineering and Industrial Aerodynamics*, 80:121–136, 1999.

[56] Wu Y.T., Porté-Agel F. Large-eddy simulation of wind-turbine wakes: Evaluation of turbine parametrisations. *Boundary-Layer Meteorology*, 138(3):345–366, 2011.

[57] Xie Z.T., Castro I.P. Efficient generation of inflow conditions for large eddy simulation of street-scale flows. *Flow, Turbulence and Combustion*, 81(3):449–470, 2008.

[58] Zasso A., Bottasso C.L., Schito P. *Wind turbine testing in boundary layer wind tunnel*. 1^{st} Wind Turbine Technology Forum – Venezia, Italy, 2011. Conference Proceedings.

[59] Zasso A., Rocchi D., Schito P. *Experimental and numerical study of the flow around a low rise building (CC)*. 5^{th} European & African Conference on Wind Engineering – Firenze, Italy, 2009. Conference Proceedings.

[60] Zasso A., Schito P., Bottasso C.L., Croce A. Aero-servo-elastic design of wind turbines: Numerical and wind tunnel modeling. *Environmental Wind Engineering and Design of Wind Energy Structures*, Baniotopoulos C., Borri C., Stathopoulos T.:594–619, 2011.

Investigation on the relation between incoming wind characteristics and surface pressure distribution

Daniele Rocchi, Paolo Schito, Alberto Zasso

The analysis of the unsteady pressures focusing on the extreme events has been carried out since July 2008. The study consist on an experimental wind tunnel campaign, at the Politecnico di Milano Wind Tunnel, on the scaled model of the "Cultural Center" that is under construction in Abuja (Nigeria).

CFD calculations have been conducted on the building in order to evaluate the pressure loads on the building using a RANS approach. Preliminary results have been presented by Zasso, Rocchi and Schito [59] at the 5^{th} European & African Conference on Wind Engineering (EACWE) that has been organized in Firenze (Italy) in July 2009. Mean values of pressure loads have been obtained with a satisfying accuracy by RANS simulations, while a LES approach gives the best results.

The study continues with the LES calculations on the building, using different boundary conditions and numerical models presented by Rocchi, Schito and Zasso [45] at the 5^{th} International Symposium on Computational Wind Engineering (CWE) organized in Chapel Hill (North Carolina) in May 2010.

The final results have been presented by Rocchi, Schito and Zasso [46] in the 13^{th} International Conference of Wind Engineering (ICWE) organized in Amsterdam (The Netherlands) in July 2011. The work has been selected for a Journal publication in the *ICWE Special Issue* of the *Journal of Wind Engineering and industrial Aerodynamics*. In the following pages is reported the paper submitted for publication.